Investigation of High-Speed Long-Haul Fiber-Optic Transmission

Investigation of High-Speed Long-Haul Fiber-Optic Transmission

By

Dong Yang

ECE Dept, McMaster University

A Thesis
Submitted to the School of Graduate Studies
in Partial Fulfilment of the Requirements
for the Degree
Masters in Applied Science

McMaster University
by Dong Yang, August, 2006

DEGREE (YEAR)
Electrical and Computer Engineering

McMaster University
Hamilton, Ontario

TITLE: Investigation of High-Speed Long-Haul Fiber-Optic Transmission

AUTHOR: Dong Yang, B. E. (University of Science and Technology of China)

SUPERVISOR: Dr. Shiva Kumar

NUMBER OF PAGES: 10, 53

Abstract

With the increasing demand for data rate and transmission distance, the trend in fiber-optic communications is to build an ultra-high, long-haul transmission system. One of the challenges in this kind of systems comes from the fiber dispersion and dispersion slope. For the wide-band wavelength-division multiplexing (WDM) system or ultra-high bit rate optical time-division multiplexing (OTDM) system, the dispersion slope could be a serious problem to impair the system performance.

Many studies have shown that the dispersion and dispersion slope affect the long-haul fiber transmission dramatically, especially for the high-capacity systems. Most of them recommend to totally compensate the dispersion and the dispersion slope simultaneously. And a lot of compensating techniques are proposed. However, it is not easy to realize the simultaneous compensation for the dispersion and dispersion slope in the practical systems. Therefore, the necessity of compensating the dispersion slope in wide-bandwidth systems should be verified.

We focus on the study of ultra-high bit rate (160-Gb/s) single-channel fiber-optic transmission. The results show that the dispersion slope is not necessary for the dispersion-managed system when the optimal launch parameters are given. Then we present how to find out the optimum in fiber-optic systems and a novel optimizing technology, space mapping technology (SM) is introduced, which has been successfully applied to the electromagnetic area. An application of SM in optical systems is implemented. By using this smart optimization technique, lots of computational efforts for evaluating the fine model in optimization process are saved.

Acknowledgement

I would like to thank my supervisor, Dr. Shiva Kumar, whose instruction to make this work completed smoothly. I appreciate his insightful advices, brilliant ideas and constant encouragement very much. I would also like to thank Dr. Aleksandra Boskovic in Corning Incorporated NY., and her companions for their financial support and technical discuss.

So many thanks to Cheryl Gies, Helen Jachna and Frances at Electrical and Computer Engineering Department for their kindly help.

Finally, I give my deepest gratitude and love to my wife, my parents and my sister for their supporting, believing and loving me all the time.

Contents

List of Figures

List of Tables

List of Abbreviations

WDM	Wavelength-Division Multiplexing
OTDM	Optical Time-Division Multiplexing
SOD	Second-Order Dispersion
TOD	Third-Order Dispersion
DCF	Dispersion Compensating Fiber
DSC	Dispersion Slope Compensator
OTDM	Optical Time-Division Multiplexing
SSMF	Standard Single-Mode Fiber
NZDSF	Nonzero Dispersion-Shifted Fiber
SM	Space Mapping
ISM	Implicit Space Mapping
OSM	Output Space Mapping

Chapter 1

Introduction

With the rapid progress of optical communications, many new types of fibers and optical fiber based devices are laid. All these make fiber-optic transmission reach a higher stage. In particular, the advent of the optical amplifier, such as erbium-doped fiber amplifier (EDFA), allows longer transmission distance in optical systems. The gain of the optical amplifier compensate the fiber loss and hence, the loss was not a limiting factor for the optical fiber communication systems any more. Thereafter, higher capacity system became the new focus. As the bandwidth increases, the higher-order dispersion could be a major limiting factor. Many dispersion compensation techniques have been proposed and their advantages and disadvantage were discussed. Until now, the perfect compensation for the dispersion and dispersion slope simultaneously is still an uncomplete task.

Generally, the compensation for dispersion slope is recommended for the high-speed systems due to the wider bandwidth. The standard single-mode transmission fiber has an anomalous dispersion with a positive dispersion slope, however, it is very hard to design a dispersion compensating fiber with a normal dispersion and negative dispersion slope. Thus, we need to verify that if it is a must to compensate the dispersion slope in practical optical communication systems.

The purpose of this work is to investigate the impact of dispersion and dispersion slope for a 160-Gb/s single-channel fiber-optic transmission system. We compare different

system schemes and find out that dispersion slope is not necessary to be compensated for a dispersion-managed optical fiber system if the optimal launch parameters are given. Considering that the direct optimization is a time-consuming work, we then introduce space mapping technology, an advanced optimization method, into optical communication system. An application of SM in fiber-optic transmission is implemented. The results show that the optimization time can be effectively reduced by using SM.

A brief outline of this thesis is as follows: in chapter 2, we review the dispersion compensation techniques in long-haul fiber-optic systems. The impact of dispersion slope and compensation schemes for higher-order dispersion are investigated. Chapter 3 presents our simulation results for 160-Gb/s single-channel fiber-optic transmission systems and the system performance for different system schemes is compared. Chapter 4 implements space mapping (SM) technique in long-haul, high-speed optical communication systems. Lastly, the conclusions drawn from this work are summarized in chapter 5.

Chapter 2

Background

In this chapter, we will review the evolution of the fiber-optic communication in the past couples of years, especially focusing on the limiting factors, such as fiber dispersion and dispersion slope, when the bit rate goes up to 40-Gb/s or higher in the long-haul fiber links. Thereafter, we will introduce a novel optimization technology - Space Mapping Technology (SM), which has been successfully used in microwave areas. The basic concept of SM is given and some typical SM algorithms are presented.

2.1 Evolution and Limitation of High-Speed, Long-Haul Fiber-Optic Links

During the past 20 years, the single-channel bit rate for the fiber-optic transmission systems has moved from 2.5-Gb/s to 10-Gb/s. And recently, 40-Gb/s and even higher bit rate like 160-Gb/s systems are investigated. With the increasing of the bit rate, the dispersion (the second-order dispersion, SOD) and dispersion slope (the third-order dispersion, TOD) along with the nonlinearity of optical fibers become the leading limiting factors in fiber-optic transmission systems. Therefore, the particular fibers manufactured to compensate SOD and TOD appear and the different compensation schemes are reported.

2.1.1 Review of Dispersion Compensation in Long-Haul Fiber-Optic Systems

Due to the shorter pulse duration in ultrahigh bit rate systems, the output signal will be broadened rapidly and widely after fiber propagation, which leads to overlapped intra-channel pulses. Combined with the nonlinearity of optical fiber, the system performance will degrade drastically. Hence, in the high-speed, long-haul fiber-optic transmission systems, the chromatic dispersion must be compensated. A variety of techniques of compensating chromatic dispersion have been proposed. Basically, the dispersion compensation can be classified as transmitter-based compensation, receiver-based compensation and fiber-based compensation. The first two compensating techniques, which use electrical processing in the transmitter and receiver respectively, are not widely utilized in the practical systems because they are not quite flexible to various optical networks. The fiber-based compensation, which uses a single-mode dispersion compensating fiber (DCF) with the negative dispersion to compensate the dispersion caused by the conventional transmission fiber with the positive dispersion, is the most reliable and widely implemented technique nowadays [1].

After fixing the dispersion compensation technique, how to set up the compensation scheme is the consequent problem. In [2] and [3], two different dispersion compensation schemes were compared, one is sequential dispersion compensation and the other is compact dispersion compensation (See Fig. 2.1). Scheme 1 shows the sequential compensation, which has a dispersion compensation span after each transmission span and scheme 2 depicts the compact dispersion compensation, which only consists of pre- and post- compensation spans. The results in [2] and [3] showed that the compact dispersion compensation scheme has better system performance than does the sequential dispersion compensation scheme. Also in these two references, it has been shown that high dispersive fiber like the standard single-mode fiber (SSMF) with dispersion $17ps/nm/km$ is superior to low dispersive fiber like the nonzero dispersion-shifted fiber (NZDSF) with dispersion $4.25ps/nm/km$. Besides these two dispersion compensation schemes, there is another one

named dispersion-managed scheme, which comprises a positive dispersion fiber (PDF) followed by a negative dispersion fiber (NDF) in each transmission span and the pre- and post- compensation fibers are set up at both ends of the total transmission link (See Fig. 2.2). Four-wave mixing (FWM) is one of the dominant nonlinear effects in high-speed optical communication systems, which leads to amplitude jitter in bit '1' slot and generates ghost pulse in bit '0' slots. By using dispersion-managed transmission scheme, it can be effectively reduced [4]. In each compensation interval, the local dispersion should be chosen as large as possible to reduce fiber nonlinearity while the average dispersion should be small to avoid the waveform distortion caused by the interaction between dispersion and SPM.

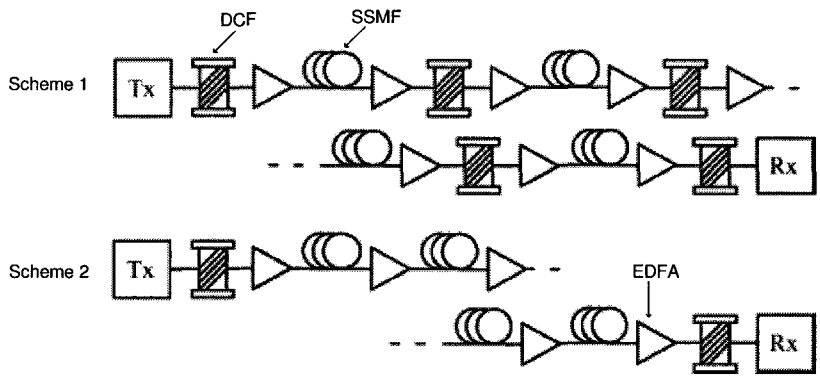

Figure 2.1: Setup of the different dispersion compensation schemes

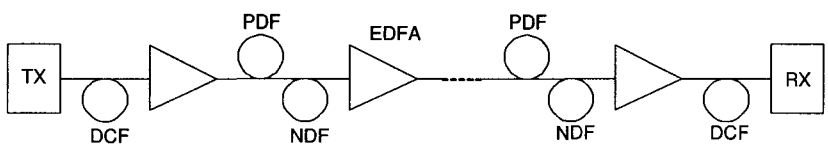

Figure 2.2: Dispersion-managed transmission system

2.1.2 Impact of Dispersion Slope in High-Speed, Long-Haul Fiber-Optic Transmission Systems

Advances in high-capacity, long-distance fiber-optic transmission makes the third-order dispersion (TOD) an important limiting factor. For example, for a wavelength-division multiplexing (WDM) system, with increasing bandwidth, it is not enough only to compensate the SOD at the particular channel, but also the TOD. Supposing that complete dispersion compensation is achieved for certain channel of the WDM system, other wavelength channels experience different amount of accumulative dispersion proportion to their wavelength separation from the zero average-dispersion wavelength channel. Consequently, the total bandwidth of the long-haul WDM system is severely limited by the fiber dispersion slope. Even if the transmission bandwidth is restricted to a single channel in high-speed ($\geq$ 160-Gb/s) optical time-division multiplexing (OTDM) systems, because of the quite broad signal bandwidth, the dispersion slope should still be taken into account. Several techniques have been proposed for the compensation of TOD. In [5], an arrayed waveguide grating (AWG)-based dispersion slope compensator (DSC) is described and long-distance WDM transmission experiments using DSC are implemented. In the experiment, the averaged zero-dispersion wavelength of fiber is set up to the center of the 10-channel WDM transmission window. The results show that the transmission performances of 10 WDM channels with the DSC are pretty much uniform. Whereas, the transmission performances are degraded at the edge of the WDM channels without the DSC. As a result, the adoption of the DSC can effectively improve the system performance. In [6], a technique based on the diameter-dependent shift of the dispersion minimum to realize a dispersion compensation module (DCM) in a predefined bandwidth has been proposed and this module can match arbitrary dispersion and dispersion slope requirements. Another method using a phase modulator as a DSC is studied in [7]. This dispersion slope compensator consists of a DCF, a SMF with opposite sign of the dispersion compared with the prior DCF and a phase modulator positioned between them (See Fig. 2.3). At the output of this DSC, the signal was pre-chirped and had a characteristic

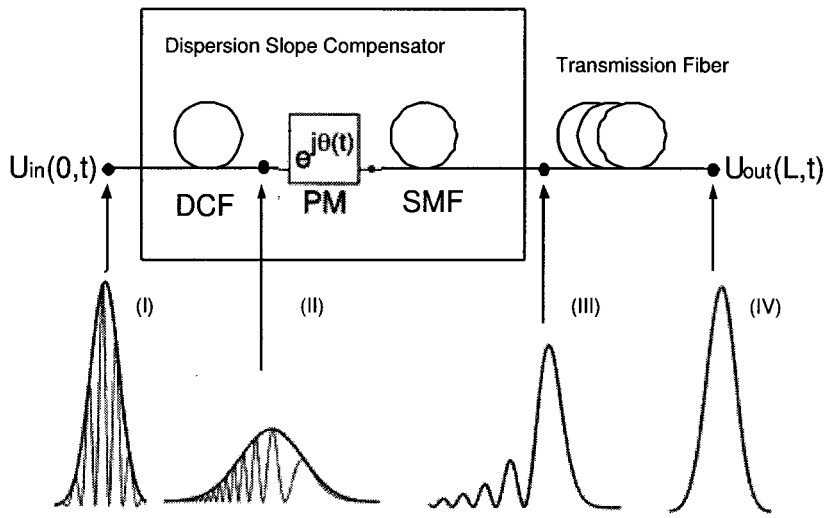

Figure 2.3: Transmission system with dispersion slope compensator. DCF: dispersion compensating fiber; PM: phase modulator; SMF: single-mode fiber. (I)input pulse, (II)linearly dispersed pulse, (III)pre-compensated pulse, (IV)fully compensated pulse.

tail induced by this chirp. Ideally, the phase shift in frequency domain induced by the third-order dispersion could be completely canceled out and hence, the dispersion slope is fully compensated at the end of fiber link. There are many other techniques or devices proposed to compensate the dispersion slope for high-speed, long-haul fiber-optic links, such as a chirped fiber Bragg grating used as a tunable DSC for a 160-Gb/s system [8], a pulse shaper with a programmable phase-modulator array used as a DSC [9], a dispersion slope equalizer using the property of fiber bending in coiled pure-silica fiber [10], and another dispersion slope equalizer using a lattice-form programmable optical filter on a planar lightwave circuit [11]. Even though so many techniques and devices have been studied for DSC, some of them are too complicated to be employed in practical systems and some are inflexible against changes in system parameters such as the number of WDM channels, the channel spacing and the signal data rate at single channel, etc.. The advent of dispersion slope compensation fiber (DSCF) made the perfect compensation for the dispersion and dispersion slope simultaneously possible and easier. This kind of DSCF

has a large normal dispersion with a negative dispersion slope [12].

On the whole, with the increasing of the bandwidth and data rate, the earliest dispersion compensation devices, with a constant dispersion across the entire transmission window, are not suitable now. The advanced devices should compensate the dispersion and dispersion slope simultaneously. Many different techniques have been proposed and these include: dispersion compensating fiber, fiber Bragg gratings based device, virtual imaged phased array based device and higher order mode dispersion compensating device [13]. Among them, the dispersion compensating fiber technique is most extensively employed nowadays.

2.2 Space-Mapping Technology

To compare various system configurations and optimize the performance, extensive numerical simulations of NLS need to be carried out. This takes several weeks to find the optimum system parameters. Therefore, in this thesis, the possibility of using space-mapping technology for optimization is explored.

Up to now, many optimization techniques for device, component, and system modeling and computer-aided design (CAD) have been used. The target of system design is to determine a set of physical parameters to satisfy certain design specifications. Traditional optimization techniques directly utilize the simulated system responses and possibly available derivatives to drive the responses to meet the design specification. However, the higher accuracy, the more expensive direct optimization is expected to be. For some complicated problems, this cost may be prohibitive. Therefore, the novel design schemes combining the accuracy with the speed in optimization are desirable and this alternative design schemes should aim for achieving a satisfactory design specification with a minimal number of computationally expensive "fine" model evaluation. Space mapping (SM) method just addressed this issue.

2.2.1 Basic SM Concept

Space-mapping technique was firstly proposed by Dr. Bandler in 1993 for design and modeling of engineering devices and systems, such as RF and microwave components by using electromagnetic (EM) simulators. The SM approach utilizes a physically based "coarse" model, which is calibrated by "fine" model, to accelerate design optimization. Here, the "coarse" model is a ideal, fast but low accuracy model, such as a low-fidelity EM simulator or an analytical model, and the "fine" model is a practical, high accuracy but computationally expensive model, such as a numerical solver based model. By constructing a SM, a proper surrogate is achieved. This surrogate is a enhanced or improved "coarse" model, which is iteratively updated and optimized in the SM procedure. The surrogate is faster than the "fine" model and more accurate than the underlying "coarse" model so that we can save a lot of efforts on evaluating the "fine" model.

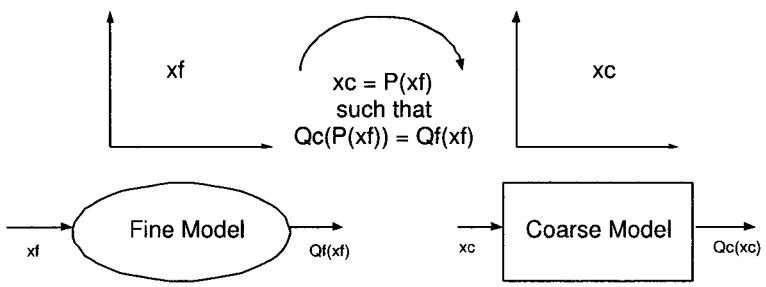

Figure 2.4: Description of the basic idea of SM

A design optimization problem to be solved can be written as [15]:

$$x^* \triangleq \arg\min_x Q(x) \tag{2.1}$$

where x is a vector of design parameters and Q is a suitable objective function. x^* is the optimal solution to be found out and it is assumed to be unique. As shown in Fig. 2.4, x_c and x_f denote the vectors of coarse and fine model design parameters, respectively. Q_c and Q_f are the corresponding objective functions or responses of coarse and fine models.

We intend to find a mapping P relating the coarse and fine model parameters as

$$x_c = P(x_f) \qquad \text{such that} \qquad Q_c(P(x_f)) \approx Q_f(x_f) \tag{2.2}$$

Then we can avoid directly optimizing the fine model, i.e., solving 2.1. Instead, we define

$$\bar{x}_f \triangleq P^{-1}(x_c^*) \tag{2.3}$$

as a good estimation of the fine-model optimum x_f^*, where x_c^* is the coarse-model optimum. Further, we assume a linear mapping is constructed between coarse and fine model design parameter spaces, i.e.,

$$x_c = P^{(j)}(x_f) = B^{(j)}x_f + c^{(j)} \tag{2.4}$$

where $B(j)$ and $c^{(j)}$ are mapping parameters at the jth iteration. A key step in SM procedure is the parameter extraction (PE) and it can be mathematically expressed as

$$\{B^{(j+1)}, c^{(j+1)}\} = \arg\min_{B,c} \| Q_f\left(x_f^{(j)}\right) - Q_c\left(P(x_f^{(j)})\right) \| \tag{2.5}$$

Then, we can obtain the optimal design parameter vector by using SM at certain iteration j+1, i.e.,

$$\bar{x}_f = x_f^{(j+1)} = \arg\min_{x_f} \left(Q_c(P^{(j+1)}(x_f))\right) \tag{2.6}$$

In general, we can summarize the SM-based optimization algorithm as follows:

step-1: Fine model evaluation.

step-2: Parameter extraction of a surrogate.

step-3: Updating the surrogate.

step-4: Optimizing the surrogate.

2.2.2 Family of Space Mapping Technology

The original SM-based optimization algorithm was proposed in 1994 [14] by Dr. Bandler, where the parameter spaces of the coarse model and fine models were linked by a linear mapping. The parameter extraction was implemented by a least square solution of the

linear equations arising from corresponding response points in the two spaces. Besides the original SM approach, there are many other enhanced or improved approaches appearing afterwards, such as Aggressive SM (ASM), Implicit SM (ISM), Neural SM (NSM) and Output SM (OSM) etc.. Considering that ISM and OSM are implemented in this work, we give particular elucidation for these two kinds of SM approaches.

2.2.2.1 Implicit Space Mapping

Generally, SM can be classified as explicit SM and implicit SM. Explicit SM constructs the mapping between the design parameter spaces of coarse and fine models, while the physical coarse model is kept fixed all the time. In contrast, implicit SM extracts the selected parameters related to the physical coarse model to match it with the fine model. Here, the mapping is established not between the design parameter spaces, but for an set of auxiliary parameters preassigned as certain physical senses. These selected preassigned parameters could be physical constants, geometrical dimensions, or mathematical concepts [16].

Given the auxiliary parameters, denoted by s, the corresponding coarse model response is $Q_c(x_c, s)$ then. At the jth iteration, the coarse-model optimal point x_c^* is given by

$$x_c^{*(j)} = \arg\min_{x_c} Q_c(x_c, s^{(j)}) \tag{2.7}$$

Then we set $x_f^{(j)} = x_c^{*(j)}$, the PE is used to find out the next iterative preassigned parameters,

$$s^{(j+1)} = \arg\min_{s} \left(Q_f(x_c^{*(j)}) - Q_c(x_c^{*(j)}, s)\right) \tag{2.8}$$

Lastly, at some iteration, like the kth iteration, we may obtain the mapped coarse model or surrogate that meets

$$Q_f(x_f) \approx Q_c(x_f, s^{(k)}) \tag{2.9}$$

over a interested region in the design parameter space. Thus, the surrogate is finally established as $Q_s(x_f) = Q_c(x_f, s^{(k)})$.

2.2.2.2 Output Space Mapping

If there is a misalignment between the optimal coarse-model response $Q_c(x_c^*)$ and the fine-model optimum $R_f(x_f^*)$, it is impossible to obtain an exact match between them. For instance, given a coarse model such as $Q_c(x_c) = x_c^2$ and a fine model $Q_f(x_f) = (2x_f - 3)^2 + 4$, we can only get a mapping $x_c = P(x_f) = 2x_f - 3$ to align them in design parameter spaces but the bias "4" between their responses is still there and can never be eliminated by any mapping P. Output space mapping (OSM) can overcome this defect by introducing a response mapping or output mapping, which is based on a Taylor extension of the coarse-model response [17].

First, we assume a linear mapping P given by

$$P(x_f) = Bx_f + c \tag{2.10}$$

where x_f is an n-dimensional vector of fine-model design parameters, B is a $n \times n$ matrix and c is an n-dimensional vector. B and c are input mapping parameters. Second, we define the output mapping as

$$O_p(z) = a(z - \bar{z}) + d \tag{2.11}$$

where a and d are OSM parameters, z is $Q_c(P(x_f))$, $\bar{z}$ is a constant, defined as $Q_c(P(\bar{x}_f))$. Assume we have reached jth iteration, let $\bar{x}_f = x_f^{(j)}$, and $d^{(j)} = Q_f(x_f^{(j)})$, then the jth surrogate can be written as

$$Q_s^{(j)}(x_f) = a^{(j)} \cdot \left(Q_c\left(P^{(j)}(x_f)\right) - Q_c\left(P^{(j)}(x_f^{(j)})\right)\right) + d^{(j)} \tag{2.12}$$

Considering that $d^{(j)} = Q_f(x_f^{(j)})$, at $x_f^{(j)}$, the surrogate $Q_s^{(j)}$ must match the fine-model response, i.e.,

$$Q_s^{(j)}(x_f^{(j)}) = Q_f(x_f^{(j)}) \tag{2.13}$$

Third, we align the current surrogate with the fine-model responses at previous iterative points by adjusting the mapping parameters $\{a, B, c, d\}$. Thus, we define a residual vector at jth iteration as

$$\mathbf{res}^{(j)}(a, B, c) = [res^{(j)}(a, B, c)_i] \tag{2.14}$$

where $res(a, B, c)_i$ stands for the ith component of the vector, given by

$$\begin{aligned} res^{(j)}(a, B, c)_i &\triangleq R_s^{(j)}(x_f^{(i)}, a, B, c) - R_f(x_f^{(i)}) \\ i &= 1, 2, \ldots, j-1 \end{aligned} \tag{2.15}$$

Finally, the residual (2.14) is used in the parameter extraction (PE) process to extract the mapping parameters for the next iteration,

$$\{a^{(j)}, B^{(j)}, c^{(j)}\} = \arg\min_{a,B,c} \|\mathbf{res}^{(j)}(a, B, c)\| \tag{2.16}$$

Chapter 3

Study of High-Speed Long Haul Fiber-Optic Links

With the increased demand for data transmission rate, the high-speed, cost-efficient fiber-optic communication systems are becoming more necessary in future optical communications. One of the usual approaches is to increase the channel count in wavelength-division-multiplexed systems (WDM). An attractive alternative is to enhance the single-channel data rate to 160-Gb/s. With the wider bandwidth at such a high bit rate, the dispersion slope has to be taken into account [21]. In general, it is recognized that the compensation for dispersion slope is required. However, considering that the dispersion slope compensating fiber is so hard to design, so we need to examine if it is definitely indispensable to compensate the dispersion slope.

Based on this concern, we numerically investigate the impact of the dispersion slope among different dispersion maps and for each map we compare the system performances between the cases with and without dispersion slope compensation. The dispersion map consisting of a single transmission fiber and the map consisting of a dispersion managed fiber are compared. It has been shown that dispersion slope compensation is not crucial for the system with dispersion managed fibers whereas, there is a significant performance degradation for the system with single transmission fiber if the dispersion slope is not

compensated. In addition, the impact of the local dispersion on fiber-optic transmission systems has also been studied. The results show that system performance improves around 0.8dB in Q with higher local dispersion ($D_+ = 17ps/(km{\cdot}nm)$, $D_- = -14.5ps/(km{\cdot}nm)$).

3.1 System Modeling and Simulations

The basic system model consists of a 160-Gb/s transmitter(Tx), transmission fiber, lumped amplifiers with a spacing of 80km, pre- and post-compensation fibers of dispersion $-100ps/(km{\cdot}nm)$ and a receiver(Rx). The operating wavelength is 1550nm and total transmission distance is 800km excluding the pre- and post-compensation fibers. In the simulation, we implement two different system schemes. In scheme 1, the transmission fiber is a dispersion managed fiber consisting of an anomalous fiber (D_+) of length 40km, followed by a normal dispersion fiber (D_-) of the same length between amplifiers (See Fig. 3.1). The scheme 2 has only the standard single mode fiber of dispersion $17ps/(km \cdot nm)$ in every amplifier span (See Fig. 3.2). The pre- and post-compensations are done by using normal dispersion fibers of dispersion $-100ps/(km \cdot nm)$. The lengths of pre- and post-compensation fibers are optimized to have the best performance.

1024-bit, chirp-free, RZ gaussian pulses with duty cycle 0.5 are used as the input signals. To study the impact of local dispersion, we further divide the scheme 1 into scheme 1A and scheme 1B. For scheme 1A, we choose $D_+ = 17ps/(km \cdot nm)$, $D_- = -14.5ps/(km \cdot nm)$ and for scheme 1B, $D_+ = 4ps/(km \cdot nm)$, $D_- = -1.5ps/(km \cdot nm)$. For scheme 2, the transmission fiber is a standard single mode fiber with dispersion $D_+ = 17ps/(km \cdot nm)$.

At the receiver, the signal is detected by a photo-diode and filtered by an electrical filter whose bandwidth is optimized. In our simulation, the amplifier noise is taken into account and the noise figure is 5.5dB for all amplifiers. We have used the Q factor defined by [22]

$$Q(dB) = 10log_{10}\left(\frac{I_1 - I_0}{\sigma_1 + \sigma_0}\right) \tag{3.1}$$

as the measure of system performance. Here, I_1 and I_0 are the mean currents of bit '1' and bit '0', respectively. σ_1 and σ_0 are the standard deviations of bit '1' and bit '0', respectively.

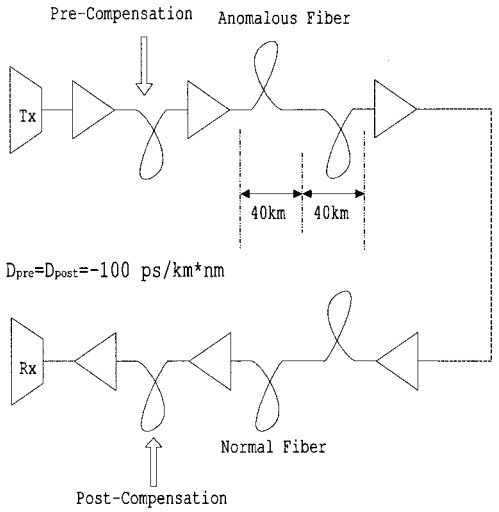

Figure 3.1: System scheme 1, the transmission fiber is a dispersion managed fiber consisting of an anomalous fiber of length 40km, followed by a normal dispersion fiber of the same length between amplifiers.

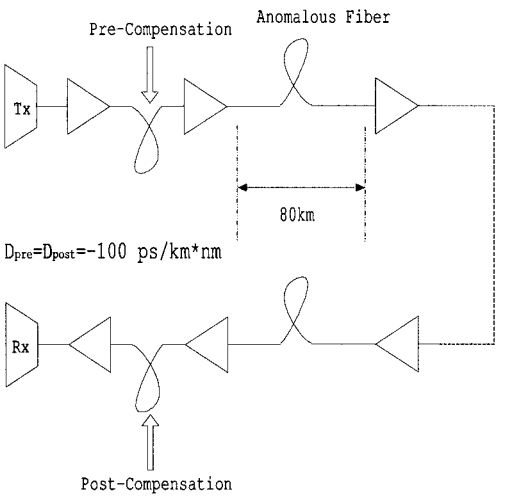

Figure 3.2: System scheme 2, with only the standard single mode fiber of length 80km between amplifiers.

3.2 Results and Discussion

To determine if the dispersion slope compensation is necessary, we have compared two kinds of system schemes. For each scheme, we first find out the optimal pre-compensation fiber length at first by fixing the launch power, then around the vicinity of this optimal value, the optimal launch power is determined.

The transmission fibers such as Single Mode Fiber (SMF) or Large Effective Area

Fiber (LEAF) have anomalous dispersion and positive dispersion slope. Since it is hard to design a normal dispersion fiber with negative dispersion slope, we first consider the dispersion slope only for the anomalous fiber, i.e., the third order order dispersion $\beta_{3anom} \neq 0, \beta_{3norm} = 0$, in the other words, the dispersion slope is not compensated. Then, we investigate the case where the dispersion slope is fully compensated, i.e., the third order dispersion $\beta_{3anom} = -\beta_{3norm} \neq 0$. Fig. 3.3(a) shows the Q factor as a function of the launch power at the optimal pre-compensation fiber length for the scheme 1 with higher local dispersion (Scheme 1A). In this picture, we can see that Q increases initially with launch power and then decreases. This can be understood by considering the relation between the launch power and noises. In our system, the noises include ASE noise and nonlinearity induced noise. σ_{ASE} is proportional to $\sqrt{P_0}$ and σ_{NL} is proportional to P_0^2. When the launch power is small, the ASE noise dominates so that $Q \sim \sqrt{P_0}$. As the launch power increases, the noise due to fiber nonlinearity will play a dominant role and therefore Q scales as $1/P_0$. We find that the optimal launch power becomes larger for the β_3 uncompensated case. This uncompensated dispersion slope leads to more broadened pulse than the β_3 compensated case so that the nonlinear effect is reduced [23]. Moreover, at the optimal point of the launch power, nearly the same Q factors are achieved. That means even if there is no compensation for the dispersion slope, we can still obtain roughly the same system performance as that with dispersion slope compensation. Considering that it is difficult to make the dispersion slope compensating fiber, our results imply that the dispersion slope compensation is not necessary if dispersion managed fibers are used. Fig. 3.3(b) shows the variations of Q as a function of pre-compensation fiber length at the optimized launch power. The optimum dispersion compensation at the transmitter for the β_3 compensated case is 80% and it decreases to 50% for the β_3 uncompensated case. This can be explained by noting that the extra high order dispersion changes the dispersion map so that the compensation scheme changes accordingly. Fig. 3.4 shows numerical results for scheme 1 with lower local dispersion (Scheme 1B) and we can find that there is a small drop in Q ($\sim 0.8dB$) when the local dispersion is lower.

Fig. 3.5 shows the effect of third order dispersion on the scheme 2. For the β_3 compensated case in scheme 2, the dispersion slope is fully compensated by pre- and post-compensation fibers. This is implemented by setting $\beta_{3pre} = \beta_{3post}$ and $\beta_{3pre} * L_{pre} + \beta_{3post} * L_{post} = -\beta_{3anom} * L$, where L_{pre} and L_{post} are lengths of pre- and post-compensation fibers and L is the total transmission fiber length. In this case, we find that the system performance degrades remarkably for the β_3 uncompensated case (1.8dB drop in Q) compared with the β_3 compensated case whereas, for scheme 1, there is no much difference in the performance between the cases with and without dispersion slope compensation. In order to explain this phenomenon clearly, we introduce three parameters [18]:

$$L_D = \frac{T_0^2}{|\beta_2|}, \qquad L'_D = \frac{T_0^3}{|\beta_3|}, \qquad L_{NL} = \frac{1}{\gamma P_0} \tag{3.2}$$

where L_D is dispersion length, L'_D is third-order dispersion length and L_{NL} is nonlinear length, these are the length scales over which the dispersive or nonlinear effects become important for pulse evolution along a fiber of length L. Based on our 160-Gb/s system with bit period, $T = 6.25ps$ and duty cycle 0.5, we can get $T_0 = (0.5 * T)/1.665 = 1.877ps$. In the simulation, we use a typical value $\beta_3 = 0.11ps^3/km$, then $L'_D = 60km$. For scheme 2, the fiber length L of every segment is $80km$ so that $L > L'_D$, while for scheme 1, L is $40km$, then $L < L'_D$. Moreover, the accumulated third-order dispersion for scheme 2 is $\beta_3 * 80km * 10$, much larger than $\beta_3 * 40km * 10$ for scheme 1. Hence, for the β_3 uncompensated case of scheme 2, the performance decreases more than that in scheme 1.

Lastly, we study the impact of local dispersion on the transmission performance and find that the system performance improve slightly for the schemes with higher local dispersion. This can be seen by comparing Q between scheme 1A and scheme 1B. Since the lower local dispersion corresponds to larger L_D and therefore, nonlinear impairments increase which degrades the system performance [20].

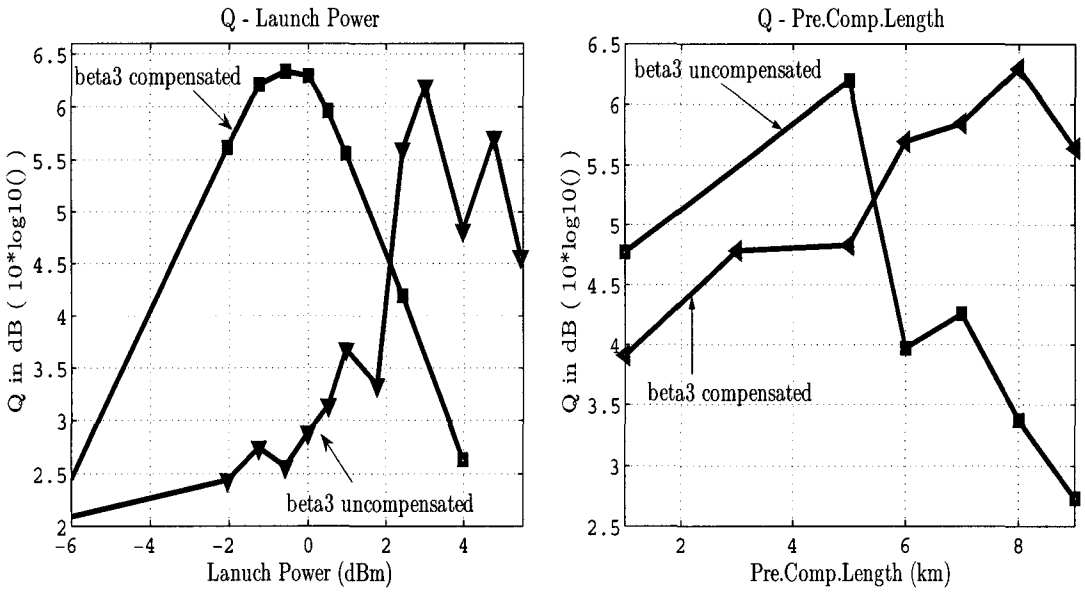

(a) (b)

Figure 3.3: Scheme 1 with higher local dispersion, $D_+ = 17ps/(km \cdot nm), D_- = -14.5ps/(km \cdot nm)$. (a)Q vs. launch power, optimal pre-compensation fiber length=8km, 5km for the β_3 compensated and β_3 uncompensated cases respectively. (b)Q vs. pre-compensation fiber length, optimal launch powers are 0dBm and 3dBm for the β_3 compensated and β_3 uncompensated cases respectively.

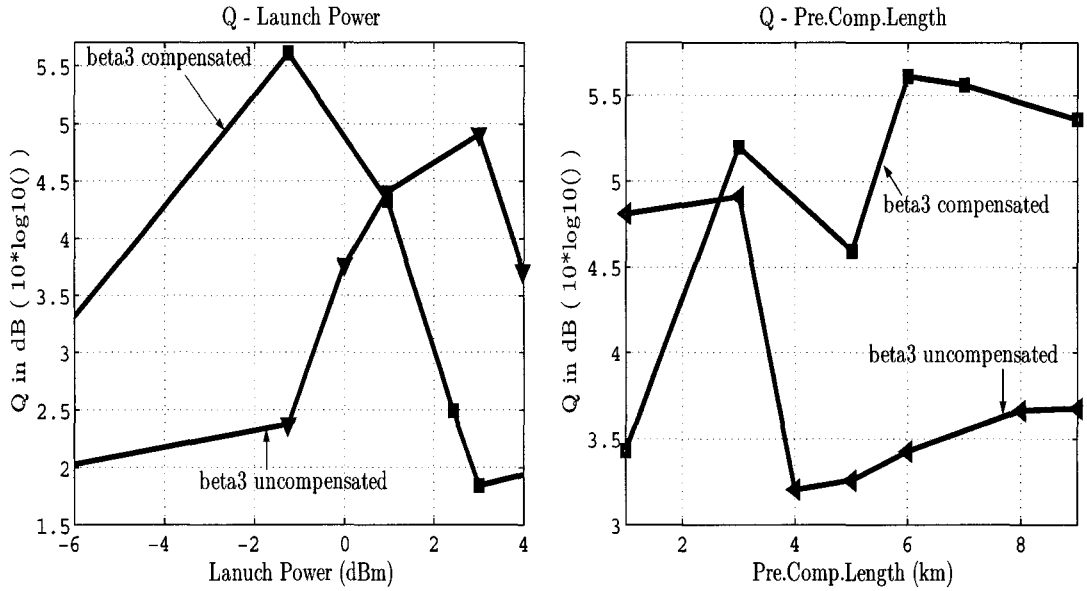

(a) (b)

Figure 3.4: Scheme 1 with lower local dispersion, $D_+ = 4ps/(km{\cdot}nm), D_- = -1.5ps/(km{\cdot}nm)$. (a)Q vs. launch power, optimal pre-compensation fiber length=6km, 3km for the β_3 compensated and β_3 uncompensated cases respectively. (b)Q vs. pre-compensation fiber length, optimal launch powers are -1.25dBm and 3dBm for the β_3 compensated and β_3 uncompensated cases respectively.

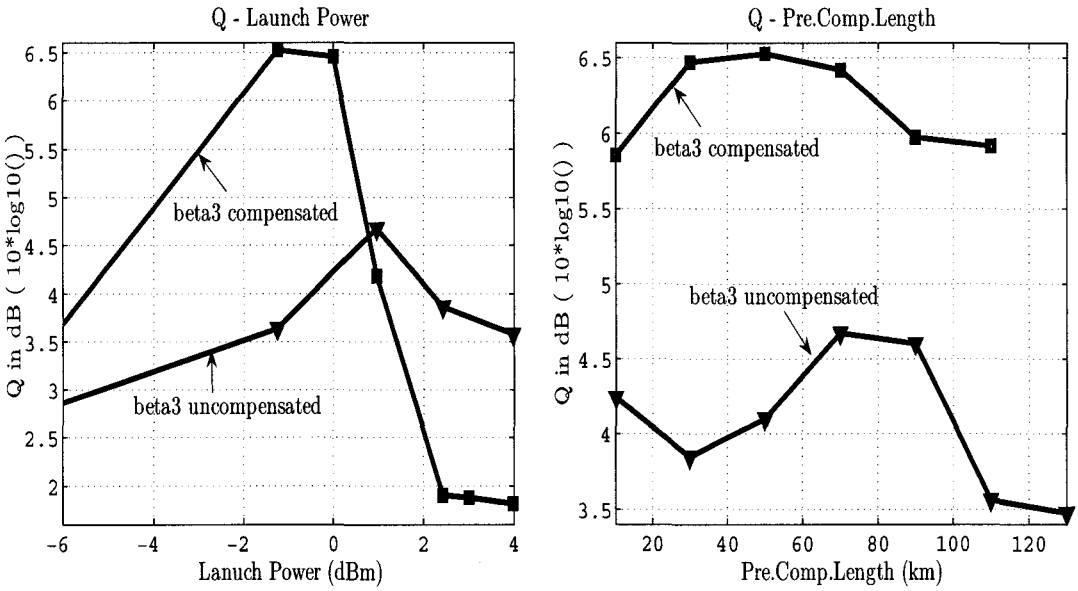

(a) (b)

Figure 3.5: Scheme 2 with dispersion, $D_+ = 17ps/(km \cdot nm)$. (a)Q vs. launch power, optimal pre-compensation fiber length=50km, 70km for the β_3 compensated and β_3 uncompensated cases respectively. (b)Q vs. pre-compensation fiber length, optimal launch powers are -1.25dBm and 0.97dBm for the β_3 compensated and β_3 uncompensated cases respectively.

3.3 Optimization Problem

In this chapter, we have found that for the system scheme 1, if the optimal input design parameters (here, they are the launch power and pre-compensation fiber length) are initially given, nearly the same system performances for the third-order dispersion compensated and uncompensated cases can be obtained. Therefore, before the simulation to get the Q factor, we first have to find the optimal design parameters, which is a optimization problem.

In our simulations, all the numerical results are obtained based on a simulator that numerically solves Nonlinear Schrodinger Equation (NLS) and we call it "fine model". And the split-step Fourier algorithm is used in this solver. The step size Δz must be less than $\phi_{max}/(\gamma P_0)$ to guarantee the computational accuracy, where ϕ_{max} is the maximal-allowed nonlinear phase shift, γ is the nonlinear coefficient and P_0 is the launched peak power. Normally, with the practical fiber transmission parameters, Δz is very small compared with the transmission length and hence, the evaluation of the fine model takes so much time. Therefore, the direct optimization of the fine model to get the optimal design parameters is computationally expensive.

In chapter 4, we apply the Space-Mapping (SM) technology to the fiber-optic transmission systems to solve this time-consuming optimization problem. The elapsed optimization time can be dramatically reduced by this technique while comparatively accurate optima can be obtained.

Chapter 4

Optimization Of the Long Haul Fiber-Optic Transmission Systems Using Space-Mapping Technology

In Chapter 3, it has been shown that the system performance for the third-order dispersion (β_3) uncompensated fiber-optic transmission system is as good as that of β_3 compensated case if the optimal input parameters are given initially. However, it is an arduous task to get the optimum of the fine model. In this chapter, we will implement a trial application by using space-mapping technology on fiber-optic transmission systems to solve the time-consuming problem when directly optimizing the fine model.

4.1 Motivations

The direct optimization of the fine model will consume lots of time and with increasing of the number of design parameters, it could be a prohibitive task to get the optima by directly optimizing the fine model. Considering such a tough time-consuming problem, we need to find an alternative way to avoid optimizing the fine model directly while getting the accurate optima. Space-mapping technology provides us a good solution to

this problem. First, space-mapping method has high efficiency to converge to optimal values by reducing evaluations of the fine model. Second, if the algorithm used in space mapping is stable enough, it will give comparatively accurate results that are nearly same as those got from direct optimization of the fine model. Even at the worst case, space-mapping method can give a good initial guess for direct optimization, which will also save much searching time.

4.2 Coarse Model

To implement the space-mapping technique, we should have a fine model (slow but high fidelity) and a coarse model (fast but low fidelity) beforehand. The fine model can be set up by a simulator that numerically solves Nonlinear Schrödinger Equation (NLS) and it gives a rigorous description of the optical signal evolution along fibers. Correspondingly, we have a coarse model as a counterpart, which is obtained based on the first-order perturbation technique.

4.2.1 First-Order Perturbation Theory

We develop a first-order perturbation technology for the study of self-phase modulation (SPM), cross-phase modulation (XPM) and four-wave mixing (FWM) effects in optical fibers. It is assumed that the pulse is linear to the leading order and nonlinearity is treated as a perturbation. The pulse propagation in optical fiber is described by Nonlinear Schrödinger Equation (NLS) [20]

$$j\frac{\partial q}{\partial z} - \frac{\beta_2(z)}{2}\frac{\partial^2 q}{\partial T^2} + \gamma_0|q|^2 q = -j\frac{\alpha(z)}{2}q, \tag{4.1}$$

where q is the electric field envelope, $\beta_2(z)$ is the dispersion profile, γ_0 is nonlinear coefficient and $\alpha(z)$ is the fiber loss/gain profile. Using the transformation,

$$q(z,T) = \exp\left(-\frac{w(z)}{2}\right)u(z,T), \tag{4.2}$$

where $w(z) = \int_0^z \alpha(s)ds$. (4.1) can be rewritten in the lossless form as

$$j\frac{\partial u}{\partial z} - \frac{\beta_2(z)}{2}\frac{\partial^2 u}{\partial T^2} + \gamma(z)|u|^2 u = 0 \tag{4.3}$$

where $\gamma(z) = \gamma_0 \exp[-w(z)]$. Without loss of generality, we consider the interaction between a pulse in bit slot 0 and a pulse in bit slot -1 to derive perturbation solutions for SPM and XPM effects. The total field can be expressed as

$$u = u_0 + u_{-1} \tag{4.4}$$

where u_0 and u_{-1} are the pulses in bit slot 0 and bit slot -1 respectively. Substituting (4.4) in (4.3) and ignoring the four-wave mixing terms, we obtain

$$j\frac{\partial u_m}{\partial z} - \frac{\beta_2(z)}{2}\frac{\partial^2 u_m}{\partial T^2} = -\gamma(z)\left[|u_m|^2 + 2|u_n|^2\right] u_m, \qquad m = 0, -1, \quad \text{and} \quad n = -1 - m. \tag{4.5}$$

We assume that the leading order solution of (4.5) is linear and treat the nonlinear terms appearing on the righ-hand side as perturbations. When fiber nonlinearity is ignored in (4.5), the field u_0 is given by [18]

$$u_0^{(0)}(z,T) = \frac{\sqrt{P_0}T_0}{T_1}\exp\left[-\frac{T^2}{2T_1^2}\right] \tag{4.6}$$

where

$$T_1 = \left(T_0^2 - jS(z)\right)^{1/2} \tag{4.7}$$

$S(z)$ is the accumulated dispersion given by

$$S(z) = \int_0^z \beta_2(s)ds \tag{4.8}$$

T_0 is the half-width at the $1/e$-intensity point [18], P_0 is the peak power of launched signals and the superscript "(0)" indicates that this is the zeroth-order solution. Similarly, we take the unperturbed field of a pulse in bit slot -1 as

$$u_{-1}^{(0)}(z,T) = \frac{\sqrt{P_0}T_0}{T_1}\exp\left[-\frac{(T+T_b)^2}{2T_1^2}\right] \tag{4.9}$$

where T_b is the bit period.

We take γ_0 as a small parameter and expand the field u_m into a series

$$u_m = u_m^{(0)} + \gamma_0 u_m^{(1)} + \gamma_0^2 u_m^{(2)} + \cdots \quad m = 0, -1 \tag{4.10}$$

where $u_m^{(k)}$ denotes that the kth-order solution at bit slot m. The zeroth-order solutions given by (4.6) and (4.9) satisfy the linear part of (4.5). Substituting (4.10) into (4.5) and collecting all the items that proportional to γ_0, we obtain

$$j\frac{\partial u_m^{(1)}}{\partial z} - \frac{\beta_2(z)}{2}\frac{\partial^2 u_m^{(1)}}{\partial T^2} = -\exp[-w(z)] \times [|u_m^{(0)}|^2 + 2|u_n^{(0)}|^2]\ u_m^{(0)},$$
$$m = 0, -1, \quad \text{and} \quad n = -1 - m. \tag{4.11}$$

To solve (4.11), we first derive the following identity. Consider a differential equation

$$j\frac{\partial f}{\partial z} - \frac{\beta_2(z)}{2}\frac{\partial^2 f}{\partial T^2} = F(z, T) \tag{4.12}$$

where the forcing function $F(z, T)$ is of the form

$$F(z, T) = \eta(z) \times \exp\left\{ -\sum_{l=1}^{2}[T - C_l(z)]^2 R_l(z) - j\kappa(z)T \right\} \tag{4.13}$$

The solution of (4.13) is given by (see Appenix A)

$$\begin{aligned} f(z, T) &= -j\int_0^z \frac{\eta(s)}{\sqrt{\delta(z, s)R(s)}} \\ &\quad \times \exp\left[-\bar{R}(C_1 - C_2)^2 + \frac{\kappa A(\kappa + j4\bar{C}R)}{4R\delta} \right] \\ &\quad \times \exp\left[-\frac{(T - \bar{C})^2 R + j\kappa T}{R\delta} \right] ds \end{aligned} \tag{4.14}$$

where

$$\begin{aligned} R &= R_1 + R_2 \\ \bar{R} &= \frac{R_1 R_2}{R_1 + R_2} \\ \bar{C} &= \frac{C_1 R_1 + C_2 R_2}{R_1 + R_2} \\ \delta &= \frac{1 - jRA}{R} \\ A &= 2[S(z) - S(s)] \end{aligned} \tag{4.15}$$

To find the first-order correction for u_0 due to the XPM term, $|u_{-1}^{(0)}|u_0^{(0)}$ in (4.11), we make use of the result given by (4.14). The forcing function $F(z,T)$ in this case is

$$\begin{aligned} F(z,T) &= -2\exp[-w(z)]|u_{-1}^{(0)}|^2 u_0^{(0)}, \\ &= 2P_0\sqrt{P_0}\eta(z)\exp\left\{-\sum_{l=1}^{2}[T-C_l(z)]^2 R_l(z)\right\} \end{aligned} \tag{4.16}$$

where

$$\eta(z) = \frac{-T_0^3\exp[-w(z)]}{T_1(z)|T_1(z)|^2}, \quad C_1(z)=0, C_2(z)=-T_b \tag{4.17}$$

$$R_1 = \frac{1}{2T_1^2}, \quad R_2 = \frac{1}{2T_2^2} = \frac{T_0^2}{|T_1(z)|^4} \tag{4.18}$$

Using (4.14), the first-order correction for u_0 due to XPM is given by

$$\begin{aligned} u_0^{(1),XPM}(z,T) = 2P_0^{3/2}\int_0^z \frac{G_1(s)}{\sqrt{\delta(z,s)R(s)}} \\ \times\exp\left[-\frac{T_b^2}{2(T_2^2+T_1^2)} - \frac{1}{\delta}\left(T-\frac{-T_b}{2RT_2^2}\right)^2\right]ds \end{aligned} \tag{4.19}$$

where

$$\begin{aligned} G_1(s) &= \frac{jT_0^3\exp[-w(s)]}{T_1(s)|T_1(s)|^2} \\ R(s) &= R_1(s)+R_2(s) = \frac{T_1^2(s)+T_2^2(s)}{2T_1^2(s)T_2^2(s)} \\ \delta(z,s) &= \frac{1-2j[S(z)-S(s)]R(s)}{R(s)} \end{aligned} \tag{4.20}$$

The first-order correction for u_0 due to the SPM term, $|u_0^{(0)}|^2 u_0^{(0)}$, can be easily obtained from (4.19) by setting T_b to 0 and by replacing the XPM factor 2 with SPM factor 1, i.e.,

$$u_0^{(1),SPM}(z,T) = P_0^{3/2}\int_0^z \frac{G_1(s)}{\sqrt{\delta(z,s)R(s)}}\exp\left(-\frac{T^2}{\delta}\right)ds \tag{4.21}$$

Total first-order solution for u_0 is obtained by adding the SPM and XPM contributions

$$\begin{aligned} u_0^{(0)}(z,T) &= P_0^{3/2}\sum_{k=0}^{1}(k+1)\frac{G_1(s)}{\sqrt{\delta(z,s)R(s)}} \\ &\quad\times\exp\left[-\frac{kT_b^2}{2(T_2^2+T_1^2)} - \frac{1}{\delta}\left(T-\frac{k(-T_b)}{2RT_2^2}\right)^2\right]ds \end{aligned} \tag{4.22}$$

Similarly, the first-order correction for u_{-1} can be obtained in the same way.

4.2.2 General Analytical Formula for the FWM Effect

So far, we have obtained the explicit solutions for SPM and XPM effects by using the perturbation theory, now we will derive the general analytical formula for the FWM effect.

Considering that the input data sequences can be expressed as:

$$u(0,T) = \sum_i u_i \tag{4.23}$$

where

$$u_i = \sqrt{P_0}\exp\left[-\frac{(t-iT_b)^2}{2T_0^2}\right] \tag{4.24}$$

is the input signal at the *i-th* bit slot. The signal evolution when propagating along fibers will be governed by Nonlinear Schrödinger Equation (NLS) (lossless form),

$$j\frac{\partial u}{\partial z} - \frac{\beta_2(z)}{2}\frac{\partial^2 u}{\partial T^2} + \gamma(z)|u|^2 u = 0 \tag{4.25}$$

where $\gamma(z) = \gamma_0 \exp[-w(z)]$. And by using the series of the field u with respect to γ_0,

$$u = u^{(0)} + \gamma_0 u^{(1)} + \gamma_0^2 u^{(2)} + \cdots \tag{4.26}$$

firstly, ignore the nonlinear part in (4.25), we can obtain the leading order solution for *i-th* bit,

$$u_i^{(0)}(z,T) = \frac{\sqrt{P_0}T_0}{T_1}\exp\left[-\frac{(T-iT_b)^2}{2T_1^2}\right] \tag{4.27}$$

where

$$T_1^2 = T_0^2 - jS(z) \quad \text{and} \quad S(z) = \int_0^z \beta_2(s)ds \tag{4.28}$$

Then the total zeroth order solution can be expressed as:

$$u^{(0)}(z,T) = \sum_i u_i^{(0)}(z,T) \tag{4.29}$$

Inserting (4.29) and (4.26) into (4.25), ignoring the second-order and other higher order terms and collecting all the terms that proportional to γ_0, we obtain

$$j\frac{\partial u^{(1)}}{\partial z} - \frac{\beta_2(z)}{2}\frac{\partial^2 u^{(1)}}{\partial T^2} = -\exp[-w(z)]\left|\sum_i u_i^{(0)}\right|^2 \sum_i u_i^{(0)} \tag{4.30}$$

This equation can also be rewritten as:

$$j\frac{\partial u^{(1)}}{\partial z} - \frac{\beta_2(z)}{2}\frac{\partial^2 u^{(1)}}{\partial T^2} = -\exp[-w(z)]\left(\sum_m u_m^{(0)}\right)\left(\sum_k u_k^{(0)}\right)^*\left(\sum_n u_n^{(0)}\right) \tag{4.31}$$

Then, combine these three factors, we obtain:

$$j\frac{\partial u^{(1)}}{\partial z} - \frac{\beta_2(z)}{2}\frac{\partial^2 u^{(1)}}{\partial T^2} = -\exp[-w(z)]\left(\sum_{m,n,k} u_m^{(0)}u_n^{(0)}u_k^{(0)*}\right) \tag{4.32}$$

Without loss of generality, we just consider the field in the bit slot 0. Because only the terms that meet $m+n-k=0$ will contribute to bit slot 0, (4.32) can be rewritten as

$$j\frac{\partial u_0^{(1)}}{\partial z} - \frac{\beta_2(z)}{2}\frac{\partial^2 u_0^{(1)}}{\partial T^2} = -\exp[-w(z)]\left(\sum_{m+n-k=0} u_m^{(0)}u_n^{(0)}u_k^{(0)*}\right) \tag{4.33}$$

Contrast (4.33) with (4.12), we have

$$f(z,T) = u_0^{(1)}(z,T) \tag{4.34}$$

$$F(z,T) = -\exp[-w(z)] \times \sum_{m+n-k=0} u_m^{(0)}u_n^{(0)}u_k^{(0)*} \tag{4.35}$$

where

$$\begin{aligned} u_m^{(0)} &= \sqrt{P_0}\frac{T_0}{T_1}\exp\left[-\frac{(T-mT_b)^2}{2T_1^2}\right] \\ u_n^{(0)} &= \sqrt{P_0}\frac{T_0}{T_1}\exp\left[-\frac{(T-nT_b)^2}{2T_1^2}\right] \\ u_k^{(0)} &= \sqrt{P_0}\frac{T_0}{T_1}\exp\left[-\frac{(T-kT_b)^2}{2T_1^2}\right] \end{aligned} \tag{4.36}$$

Substituting (4.36) into (4.35), for a group of definite (m,n,k), after some algebraic combination and reduction, we can obtain

$$\begin{aligned} F(z,T) &= \eta(z) \times \exp\left\{-\sum_{l=1}^{2}[T-C_l(z)]^2 R_l(z) - j\kappa(z)T\right\} \\ &= -\exp[-w(z)] \cdot P_0^{3/2} \cdot \frac{T_0^3}{|T_1|^2 T_1} \cdot \exp\left[-\frac{(m-n)^2T_b^2}{4|T_1|^4}\cdot(T_1^2)^*\right] \\ &\quad \times \exp\left[-\frac{(T-(m+n)T_b/2)^2}{2|T_1|^4}\cdot 2(T_1^2)^* - \frac{(T-kT_b)^2}{2|T_1|^4}\cdot T_1^2\right] \end{aligned} \tag{4.37}$$

where,

$$\begin{aligned}
\eta(z) &= -\exp[-w(z)] \cdot P_0^{3/2} \cdot \frac{T_0^3}{|T_1|^2 T_1} \cdot \exp\left[-\frac{(m-n)^2 T_b^2}{4|T_1|^4} \cdot (T_1^2)^*\right] \\
C_1(z) &= \frac{m+n}{2} T_b \qquad C_2(z) = kT_b \\
R_1(z) &= \frac{(T_1^2)^*}{|T_1|^4} = \frac{1}{T_1^2} \qquad R_2(z) = \frac{T_1^2}{2|T_1|^4} = \frac{1}{2(T_1^2)^*} \\
\kappa(z) &= 0
\end{aligned} \tag{4.38}$$

Lastly, we obtain the first-order correction for the field in bit slot 0 by (4.14)

$$\begin{aligned}
\Delta u(z,T)_{(m,n,k)} = -j \int_0^z & \frac{\eta(s)}{\sqrt{\delta(z,s)R(s)}} \\
& \times \exp\left[-\bar{R}(C_1 - C_2)^2\right] \times \exp\left[-\frac{(T-\bar{C})^2}{\delta}\right] ds
\end{aligned} \tag{4.39}$$

where

$$\begin{aligned}
R &= R_1 + R_2 \\
\bar{R} &= \frac{R_1 R_2}{R_1 + R_2} \\
\bar{C} &= \frac{C_1 R_1 + C_2 R_2}{R_1 + R_2} \\
\delta &= \frac{1 - jRA}{R} \\
A &= 2[S(z) - S(s)]
\end{aligned} \tag{4.40}$$

(4.39) give us a general form for nonlinear effects in the fiber propagation, which are contributed by the fields at bit slot m, n and k. If $m = n = k$, it stands for SPM effect; if $m = k$ or $n = k$ but $m \neq n$, it gives intrachannel XPM effect; excluding these two cases, it presents intrachannel FWM (IFWM) effect. As shown in Fig. 4.1, the nonlinear interaction of closely spaced pulse pairs generates temporal side bands or ghost pulses due to intrachannel FWM. The ghost pulse falling on the bit "1" slots causes amplitude jitter. Assume we have three consecutive bits of "1", centered at $-2T_b$, $-T_b$ and 0 respectively. The ghost pulse generated by the nonlinear mixing of pulses at $-2T_b$ and $-T_b$ interferes with the pulse at slot 0. This interference is added on the field on bit slot 0 and incudes amplitude jitter.

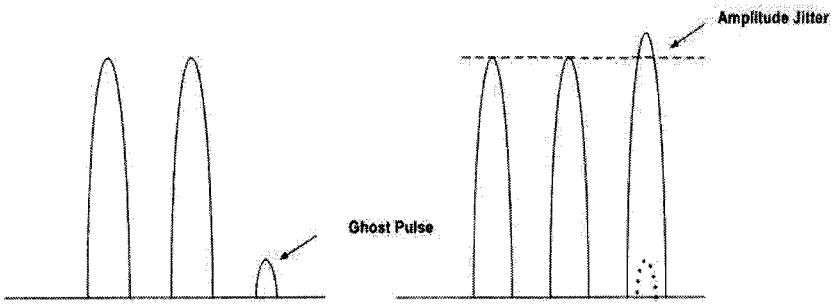

Figure 4.1: Illustration of Intrachannel FWM

Then, from (4.35), the total intrachannel FWM correction at bit slot 0 can be obtained by summing up the contributions from all the possible combinations of (m, n, k), i.e.,

$$\Delta u(z,T)_{tot}^{IFWM} = \sum_{m+n-k=0} \Delta u(z,T)_{(m,n,k)}^{IFWM} \tag{4.41}$$

4.2.3 Examining the Validity Of the First-Order Perturbation

When the dispersion length is much shorter than the nonlinear distance, we find that the first-order solution can adequately describe the nonlinear effects and so we can ignore the second and the other higher order corrections for the leading order solution.

Fig. 4.2 shows the optical power of a single pulse after 5 spans. In this case, there is a standard single mode fiber of dispersion (D_+) $4ps/(km \cdot nm)$ in each amplifier span and the amplifier spacing is 80 km. The dashed with dotted, the dashed only and the solid lines show the numerical simulation result, first-order and zeroth-order solutions.

Fig. 4.3 shows the ghost pulse appearing at bit slot 0 when input two-bit signals at bit slot -1 and bit slot -2. In this case, the transmission fiber is a dispersion managed fiber, consisting of an anomalous fiber (D_+) followed by a normal fiber (D_-). And the residual dispersion is fully compensated by pre- and post- compensation fibers of dispersion $-100ps/(km \cdot nm)$. The dashed with dotted and the dashed only lines show the numerical simulation result and the first-order solution.

For 160-Gb/s RZ systems, the pulsewidth is in the range of 1.5 to 3.1 ps. If $|\beta_2|$ is in

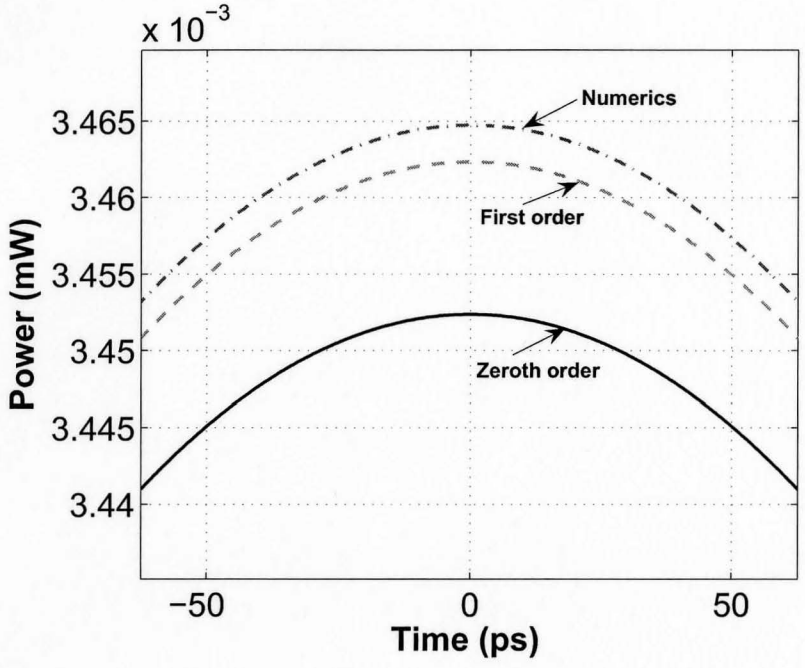

Figure 4.2: Optical power as a function of time due to SPM alone. Peak power= 2mW, D_+= 4 $ps/(km \cdot nm)$, , bit rate = 160 Gb/s, 5 spans.

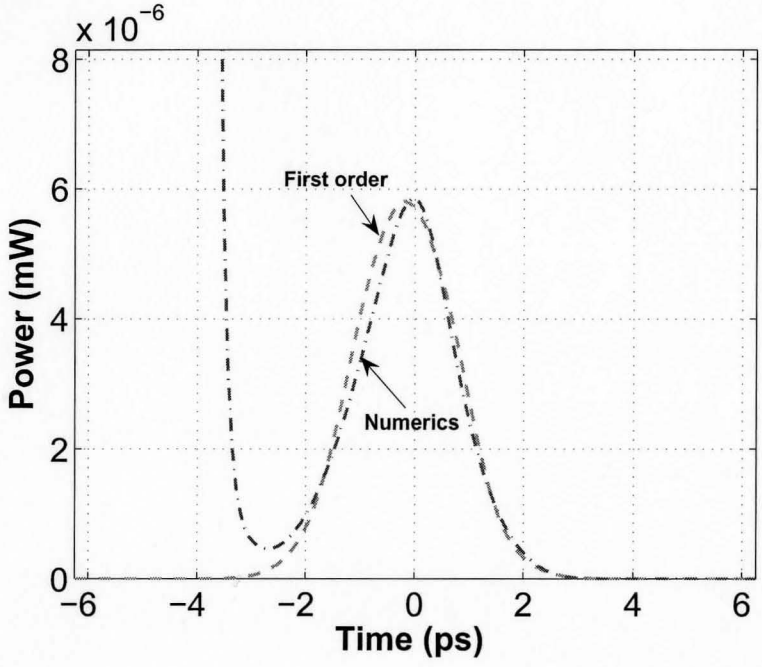

Figure 4.3: Optical power as a function of time due to IFWM. Launched two input bits at bit slot -1 and bit slot -1, watch the ghost pulse at bit slot 0. Peak power= 2mW, $D_+ = 17ps/(km \cdot nm)$, $D_- = -14.5ps/(km \cdot nm)$, bit rate= 160 Gb/s, 10 spans.

the range of 4-21ps^2/km and the dispersion length is given by

$$L_D = T_0^2/|\beta_2|, \tag{4.42}$$

then the typical dispersion length is in the range of $0.04km$ to $0.9km$. We define the nonlinear length as

$$L_{NL} = \frac{1}{\gamma_0 P_0} \tag{4.43}$$

where γ_0 is the nonlinear coefficient and P_0 is launched peak power. If taking the typical nonlinear coefficient as $2.5W^{-1}km^{-1}$, the nonlinear length is $200km$ when the launched peak power equals to $2mW$. Thus, we can find that the dispersion length is much less than the nonlinear length for 160-Gb/s RZ systems and hence, the first-order theory is adequate to describe the nonlinear effects. Fig. 4.2 and Fig. 4.3 are just showing the validity of first-order theory for SPM and IFWM effects, respectively.

4.2.4 Calculation Of the Nonlinear Noise

As for the 160-Gb/s, RZ, dispersion-managed systems, because of the smaller dispersion length, the pulses will be broadened rapidly and hence, the adjacent pulses are overlapped strongly each other. In this case, the limiting factors for the fiber transmission are the amplitude fluctuations in bit '1' slots and the ghost pulse generation in bit '0' slots, induced by intrachannel four-wave mixing (IFWM) [23].

Based on perturbation theory, we can express the field as

$$u = u_0 + \Delta u \tag{4.44}$$

where u_0 is the linear part solution of NLS and Δu can be treated as a perturbation caused by nonlinearity. Here, we only focus on the IFWM effect, so $\Delta u = \Delta u^{IFWM}$ and it is given by (4.41). Assume h_i is the probability of having bit '1' in bit slot i, which is taken as 1/2, then NLS given by (4.33) can be rewritten as

$$j\frac{\partial u_0^{(1)}}{\partial z} - \frac{\beta_2(z)}{2}\frac{\partial^2 u_0^{(1)}}{\partial T^2} = -\exp[-w(z)]\left(\sum_{m+n-k=0}(h_m h_n h_k)\, u_m^{(0)} u_n^{(0)} u_k^{(0)*}\right) \tag{4.45}$$

Further, (4.41) can be rewritten as

$$\Delta u(z,T)_{tot}^{IFWM} = \sum_{m+n-k=0} (h_m h_n h_k)\ \Delta u(z,T)_{(m,n,k)}^{IFWM} \tag{4.46}$$

and then,

$$\begin{aligned}(\Delta u(z,T)_{tot}^{IFWM})^2 &= \left(\sum_{m+n-k=0} (h_m h_n h_k)\ \Delta u(z,T)_{(m,n,k)}^{IFWM}\right)\cdot \\ &\quad \left(\sum_{o+p-q=0} (h_o h_q h_q)\ \Delta u(z,T)_{(o,p,q)}^{IFWM}\right) \\ &= \sum_{m+n-k=0} \cdot \sum_{o+p-q=0} (h_m h_n h_k h_o h_q h_q)\cdot \Delta u(z,T)_{(m,n,k)}^{IFWM}\cdot \Delta u(z,T)_{(o,p,q)}^{IFWM}\end{aligned} \tag{4.47}$$

At the end of the link, the output optical power can be written as

$$P_{out} = |u_0 + \Delta u|^2 = |u_0|^2 + u_0^*\Delta u + u_0\Delta u^* + |\Delta u|^2 \tag{4.48}$$

Assume $|\Delta u| \ll |u_0|$, ignore $|\Delta u|^2$, we obtain

$$P_{out} = P_0 + \delta P = |u_0|^2 + (u_0^*\Delta u + u_0\Delta u^*) \tag{4.49}$$

The variance of the nonlinear noise is

$$\sigma_{NL}^2 = < \delta P^2 > - < \delta P >^2 \tag{4.50}$$

where $< \cdot >$ denotes taking mean value.

$$< \delta P > = u_0^* < \Delta u > + u_0 < \Delta u^* > \tag{4.51}$$

and

$$< \delta P^2 > = u_0^{*2} < \Delta u^2 > + u_0^2 < \Delta u^{*2} > + 2|u_0|^2 < |\Delta u|^2 > \tag{4.52}$$

Then, by using (4.45) and (4.47) [19], we obtain

$$< \Delta u > \sim < m_i m_j m_k > = \begin{cases} \frac{1}{2^3} & \text{if } i \neq j \neq k \\ \frac{1}{2^{3-r+1}} & \text{if any r indices are equal} \end{cases} \tag{4.53}$$

$$< \Delta u^2 > \sim < m_i m_j m_k m_o m_p m_q > = \begin{cases} \frac{1}{2^6} & \text{if } i \neq j \neq k \neq o \neq p \neq q \\ \frac{1}{2^{6-r+1}} & \text{if any r indices are equal} \end{cases} \tag{4.54}$$

Insert (4.53), (4.54) into (4.51) and (4.52), $< \delta P >$ and $< \delta P^2 >$ are achieved. Then, the nonlinear noise variance caused by IFWM can be obtained by (4.50).

4.2.5 Calculation Of the ASE Noise

Besides the noise induced by the fiber nonlinearity, the lumped amplifiers in the transmission link introduce another noise - ASE noise. ASE noise variance is

$$\sigma_{ASE}^2 = 2R^2 \cdot P_s \cdot P_N \tag{4.55}$$

where R is the responsivity of a photodiode, P_s and P_N are signal power and noise power respectively.

$$P_s = P_{j,peak} \tag{4.56}$$

where $j = 0, 1$ for bit '0' or bit '1'.

$$P_N = \rho_{ASE} \cdot \Delta f \tag{4.57}$$

where Δf is the electrical filter bandwidth and

$$\rho_{ASE} = hf(GF - 1) \tag{4.58}$$

where f is the Planck constant, f is the operation frequency, G is the amplifier gain and F is the noise figure.

4.2.6 Establishment Of the Coarse Model

In our simulation, Q factor is taken as a measurement of system performance and the higher Q factor, the better system performance. Therefore, the objective of our optimization is to get the maximal Q factor at certain design parameters. For the coarse model, we have

$$Q_c = 10 \log_{10} \left(\frac{I_1 - I_0}{\sigma_1 + \sigma_0} \right) \tag{4.59}$$

where

$$\sigma_1 = \sqrt{\sigma_{NL1}^2 + \sigma_{ASE1}^2} \quad \text{is the standard deviation of bit '1'} \tag{4.60}$$

and

$$\sigma_0 = \sqrt{\sigma_{NL0}^2 + \sigma_{ASE0}^2} \quad \text{is the standard deviation of bit '0'} \tag{4.61}$$

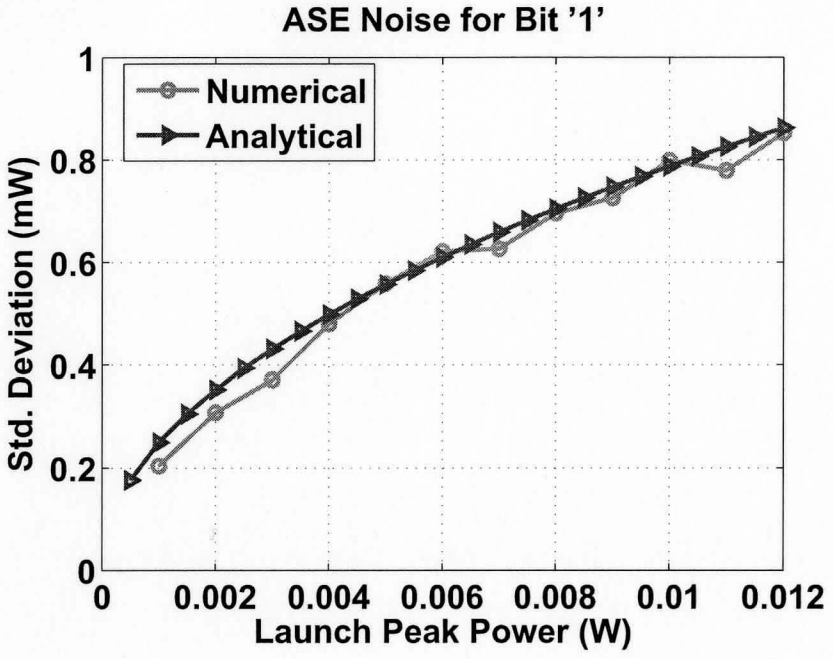

Figure 4.4: ASE noise as a function of the launched peak power

Insert (4.50) and (4.55) into (4.60) and (4.61), we can obtain the standard deviations of bit '1' and bit '0' for the coarse model. Considering that usually $I_1 \gg I_0$ and $I_1 \approx RP_0$, we can ignore I_0 in (4.59). Ultimately, the coarse model is established as

$$Q_c(x_c) = 10\log_{10}\left(\frac{I_1}{\sigma_1 + \sigma_0}\right) = 10\log_{10}\left(\frac{RP_0}{\sigma_1 + \sigma_0}\right) \tag{4.62}$$

where x_c is a vector denoting the design parameter and P_0 is the launched peak power, R is the responsivity of a photodiode.

4.3 Two-Stage Implementation Of Space-Mapping Technique

So far, we have a coarse model based on an analytical formula and a fine model based on a simulator numerically solving NLS. In the fine model, the split-step Fourier method is used and the step size Δz is dependent on the launched peak power as

$$\Delta z \leq \phi_{max}/(\gamma \cdot P_0) \tag{4.63}$$

where ϕ_{max} is the maximal allowed nonlinear phase shift. Apparently, as the launch power increases, Δz becomes smaller, then evaluation time of the fine model goes up. Whereas, the evaluation of the coarse model is nothing but calculating an integral, which is totally independent of the launched peak power. Therefore, the step size for the coarse model is fixed and could be quite large as long as the accuracy of the integration could be guaranteed. Normally, the evaluation time for the fine model is around 2.5 hours at a lower level of the launched peak power, by contrast, it is less than 3 seconds for the coarse model. On the other hand, the fine model is of higher fidelity compared with the coarse model. Space-mapping (SM) technology builds a bridge between the coarse and fine models. SM procedures iteratively update and optimize surrogates (based on a fast physically based coarse model) and then link the design parameters in the space of coarse and fine models by a mapping, given by $x_c = P(x_f)$. Here, the surrogate is a mapped coarse model or enhanced coarse model.

To implement space-mapping technique, we first assign the design parameters used in the optimization process. In our simulation, we choose the launched peak power and dispersion compensation ratio as the optimized design parameters and they are denoted by x_c and x_f for the coarse and fine models, respectively. Here, they are 2×1 vectors and $x_c(1)$, $x_f(1)$ stand for launched peak power; $x_c(2)$, $x_f(1)$ stand for dispersion compensation ratio (DCR), which is defined by

$$DCR = \frac{\text{pre-compensation fiber length}}{\text{total compensation fiber length}} \times 100\% \tag{4.64}$$

4.3.1 First Stage: Implicit Space Mapping (ISM)

Considering that the original coarse model has a large deviation from the fine model (See Fig. 4.5, 4.7), we can not use Explicit Space Mapping (such as ASM, OSM) directly. Hence, we insert an Implicit Space Mapping (ISM) to improve the original coarse model. After ISM, we get an enhanced coarse model with better approximating to the fine model. Then, we implement Output Space Mapping (OSM) to find the optimal design parameters based on this improved coarse model [16].

In ISM, a set of auxiliary parameters (selected preassigned parameters) is extracted to match the coarse model to the fine model. The total noise can be expressed as:

$$\sigma_{tot}^2 = \sigma_{NL}^2 + \sigma_{ASE}^2 \tag{4.65}$$

where σ_{NL}^2 and σ_{ASE}^2 are nonlinear noise and ASE noise variances respectively. In Fig. 4.4, it is shown that the practical ASE noise can be depicted well by the analytical formula (4.55) and so, we only need to align nonlinear noise of the coarse model with that of the fine model.

We introduce two preassigned parameters named "AdjustSigma1" and "AdjustSigma0", then obtain

$$\begin{aligned} \tilde{\sigma}_{NL1}^2 &= (\text{AdjustSigma1}) \times \sigma_{NL1}^2 \\ \tilde{\sigma}_{NL0}^2 &= (\text{AdjustSigma0}) \times \sigma_{NL0}^2 \end{aligned} \tag{4.66}$$

where σ^2_{NL1} and σ^2_{NL0} are original coarse-model outputs of the nonlinear variances for bit '1' and bit '0'; $\tilde{\sigma}^2_{NL1}$ and $\tilde{\sigma}^2_{NL0}$ are improved coarse-model. Then, for the improved coarse model, the noise can be rewritten as

$$\begin{aligned} \sigma^2_{tot1} &= \tilde{\sigma}^2_{NL1} + \sigma^2_{ASE1} \\ \sigma^2_{tot0} &= \tilde{\sigma}^2_{NL0} + \sigma^2_{ASE0} \end{aligned} \tag{4.67}$$

Further, the Q factor for the coarse model, now is given by

$$Q_c(x_c) = 10\log_{10}\frac{I_1}{\sigma_{tot1} + \sigma_{tot0}} \tag{4.68}$$

The following table presents the executable algorithm of ISM,

Table 4.1: Summary of the ISM Algorithm

Step 1	select preassigned parameters $x = [adjustsigma1; adjustsigma0]$
Step 2	Set $j = 0$ and initialize $x^{(0)}$
Step 3	Obtain the optimal coarse model design parameters by solving $x_c^{*(j)} \equiv arg\min_x \left(Q_c(x_c, x^{(j)})\right)$
Step 4	Terminate if stop criteria (e.g. $\parallel x_c^{*(j)} - x_c^{*(j-1)} \parallel < \varepsilon$) are satisfied.
Step 5	set $x_f^{(j)} = x_c^{*(j)}$
Step 6	Evaluate the fine model at $x_f^{(j)}$
Step 7	Calibrate the coarse model by extracting the preassigned parameters x by $x^{(j+1)} = arg\min_x(\parallel \sigma_f(x_f^{(j)}) - \sigma_c(x_f^{(j)}, x^{(j)}) \parallel)$ where $\sigma_f = [\sigma_{f1}; \sigma_{f0}]$ and $\sigma_c = [\sigma_{c1}; \sigma_{c0}]$
Step 8	Increase j and go to step 3

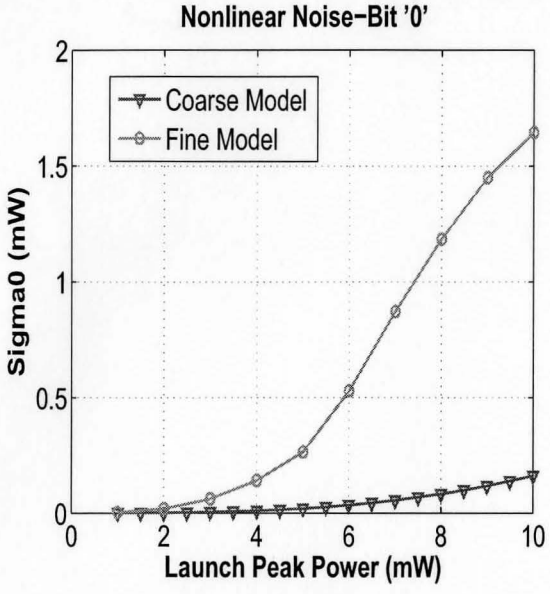

Figure 4.5: Nonlinear noise of bit '0' for the coarse model.

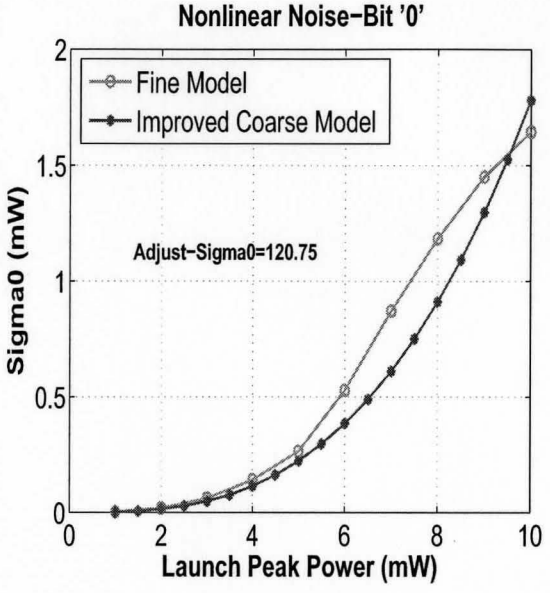

Figure 4.6: Nonlinear noise of bit '0' for the surrogate.

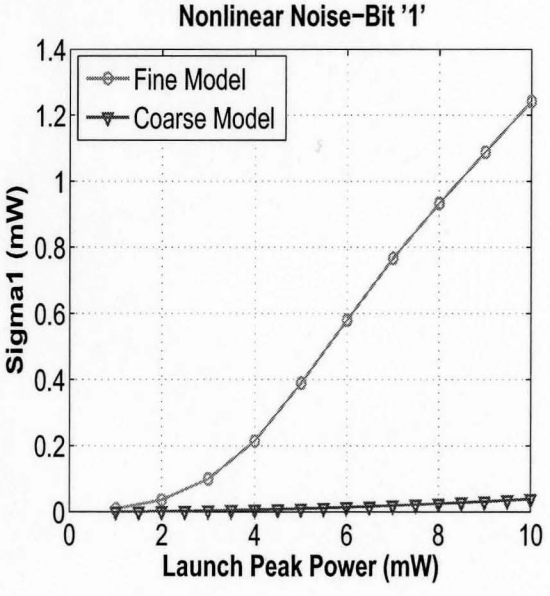

Figure 4.7: Nonlinear noise of bit '1' for the coarse model.

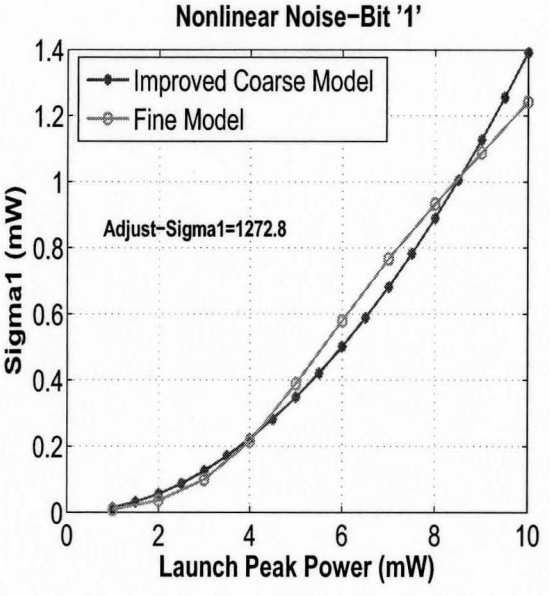

Figure 4.8: Nonlinear noise of bit '1' for the surrogate.

4.3.2 Second Stage: Output Space Mapping (OSM)

OSM deals with residual misalignment between the optimal coarse-model output and fine-model output. For example, a coarse model such as $R_c = x^2$ will never match to the fine model $R_f = x^2 - 5$ around its minimum with any mapping $x_c = P(x_f)$. Therefore, in the original SM [17], an exact match between the mapped coarse model and fine model is impossible. Output Space Mapping can overcome this deficiency by introducing a bias term in the output of the coarse model. Along with the input mapping P, OSM can give a better calibration or a better surrogate.

After ISM, we've achieved a improved coarse model with particular preassigned parameters: $[adjustsigma1; adjustsigma0] = [1272.8; 120.75]$. Based on this enhanced coarse model, we further implement the explicit space mapping (OSM) to calibrate it so that the mapped coarse model after OSM can match the fine model exactly.

Though, normally the input mapping P is nonlinear, it can be approximated by local linear mappings. We assume a linear mapping

$$P(x_f) = Bx_f + c \tag{4.69}$$

where $x_f \in \mathbb{R}^2$ is the fine-model design parameter vector, the matrix $B \in \mathbb{R}^{2\times 2}$ and $c \in \mathbb{R}^2$. The output mapping is defined as

$$O(z) = \alpha(z - \bar{z}) + \beta \tag{4.70}$$

where $\bar{z} = Q_c(B\bar{x}_f + c)$ and $\bar{x}_f$ is a constant vector. Then the surrogate can be written as:

$$Q_s(x_f) = \alpha\left(Q_c(Bx_f + c) - Q_c(B\bar{x}_f + c)\right) + \beta \tag{4.71}$$

If let $\bar{x}_f = x_f^{(j)}$ and $\beta = Q_f(x_f^{(j)})$, where $x_f^{(j)}$ is the jth iterate, then we obtain

$$Q_s^{(j)}(x_f^{(j)}) = Q_f(x_f^{(j)}) \tag{4.72}$$

at current iterative point $x_f^{(j)}$. Thus, jth iterative surrogate is

$$Q_s^{(j)}(x_f) = \alpha^{(j)}\left(Q_c(P^{(j)}(x_f)) - Q_c(P^{(j)}(x_f^{(j)}))\right) + \beta^{(j)} \tag{4.73}$$

where $P^{(j)}(x_f) = B^{(j)}x_f + c^{(j)}$ and $\beta^{(j)} = Q_f(x_f^{(j)})$. In each iteration, the surrogate is optimized to find the next iterate by solving

$$x_f^{(j+1)} = arg\min_{x_f}\left(Q_s^{(j)}(x_f)\right) \tag{4.74}$$

The mapping parameters are updated by the Parameter Extraction (PE) process and it is implemented by matching the single or multiple iterative points between the surrogate and the fine model. In our simulation, only the latest previous point is matched during the PE process, which can be mathematically expressed as:

$$\left\{\alpha^{(j+1)}, B^{(j+1)}, c^{(j+1)}\right\} = arg\min_{\alpha,B,c}\left(Q_s^{(j+1)}(x_f^{(j)}, \alpha, B, c) - Q_f(x_f^{(j)})\right) \tag{4.75}$$

Table 4.2: Proposed OSM Algorithm

Step 1	select a coarse model and fine model
Step 2	Set $j = 0$ and initialize $x_f^{(0)}$
Step 3	Obtain the the next iterate $x_f^{(j+1)}$ by solving $x_f^{*(j+1)} \equiv arg\min_{x_f}\left(Q_s^{(j)}(x_f)\right)$
Step 4	Terminate if stop criteria (e.g. $\parallel x_f^{*(j+1)} - x_f^{*(j)} \parallel < \varepsilon$) are satisfied.
Step 5	Evaluate $Q_f(x_f^{(j+1)})$
Step 6	In PE process to update the input and output mapping parameters $\left\{\alpha^{(j+1)}, B^{(j+1)}, c^{(j+1)}\right\}$ by solving $\left\{\alpha^{(j+1),B^{(j+1)}}, c^{(j+1)}\right\} = arg\min_{(\alpha,B,c)}\left(\parallel Q_s^{(j+1)}(x_f^{(j)}, \alpha, B, c) - Q_f(x_f^{(j)}) \parallel\right)$
Step 7	Set $j = j + 1$ and go to step 3

4.3.3 Results and Discussion

Since the direct optimization of the fine model is a time-consuming work and hence, space mapping is introduced to reduce evaluations of the fine model so that we can have higher

Table 4.3: ISM Implementation

Iteration	Preassigned Parameters $[adjustsigma1; adjustsigma0]$	$X_{c\_opt} \in \mathbb{R}^2$ [Peak Power; DCR]
0	[2000; 500]	[4.04e-3; 0.7757]
1	[993.36; 126.04]	[5.12e-3; 0.7757]
2	[1281.83; 170.06]	[4.76e-3; 0.7757]
3	[1273.18; 120.71]	[4.76e-3; 0.7757]

Table 4.4: OSM Implementation

Iteration	Mapping Parameters α, B, c	$X_{f\_opt} \in \mathbb{R}^2$ [Peak Power; DCR]
0	$\alpha = 1.0, c = [0; 0]$ $B = \begin{pmatrix} 1 & 0 \\ 0 & 1 \end{pmatrix}$	[4.76e-3; 0.7757]
1	$\alpha = 0.9999, c = [1.3\text{e-}3; -9.84\text{e-}3]$ $B = \begin{pmatrix} 0.9999 & 0 \\ 0 & 0.9922 \end{pmatrix}$	[3.8e-3; 0.7867]
2	$\alpha = 0.9999, c = [0.547\text{e-}3; -9.71\text{e-}3]$ $B = \begin{pmatrix} 0.9999 & 0 \\ 0 & 0.9922 \end{pmatrix}$	[4.1626e-3; 0.7867]
3	$\alpha = 0.9999, c = [0.594\text{e-}3; -9.71\text{e-}3]$ $B = \begin{pmatrix} 0.9999 & 0 \\ 0 & 0.9923 \end{pmatrix}$	[4.1626e-3; 0.7867]

Table 4.5: Complexity Comparison Among Coarse, Fine and Surrogate Models

Obj. Problem	Fine Model	Coarse Model	Surrogate	
			Surrogate-ISM	Surrogate-OSM
Optimization Techniques	"Direct Search"	"Direct Search"	"Implicit SM"	"Output SM"
Fun. Evals	43	105	3× Fine Model Evals. + 3× PE process	4× Fine Model Evals. + 3× PE process
Elapsed Time per Fun. Eval	$\sim 2.5 - 4.5$ hours	< 3 seconds	~ 2.5 hours	~ 2.5 hours
Optimal Design Parameters	[4.167e-3; 0.8087]	[12.874e-3; 0.7757]	[4.759e-3; 0.77574]	[4.163e-3; 0.7867]
Q-Factor of Fine Model	6.423 dB	1.212 dB	6.275 dB	6.421 dB
Total Elapsed Time	137.89 hours	151.29 seconds	7.6 hours	10.4 hours
			18hours	

efficiency. On the other hand, the optima we obtain from SM technique should approach the true optima derived from the fine model so as to ensure accuracy.

From Table 4.5, we can find that the coarse model is fast but not accurate; the fine model is slow but accurate. By using SM technology, evaluations of the fine model have been reduced and hence the efficiency is enhanced greatly, at the same time, through two-stage SM, we obtain a set of optimal design parameters well approximating to the true optima.

Fig. 4.9 to Fig. 4.12 show the surrogate model compared with the fine model. In these figures, it is shown that the surrogate model can give a good estimate of the optima. Especially for the DCR fixed case, the surrogate model is in good agreement with the fine model within a wide power range (1mW-6mW). Fig. 4.10 shows that when the launch peak power is greater than 4 mW, the coarse model deviates from the fine model significantly, which means that the first-order theory based analytical model can not describe the true model itself at higher power level. Whereas, the surrogate model that is modified by using the information from the fine model can track the fine model well even at the higher power level (See Fig. 4.9).

By using SM techology, we obtain two benefits. First, high efficiency: 18 hours for SM-based optimization versus 138 hours (around 5 days) for direct optimization. Second, high accuracy: the relative error, between the optimal design parameters of the surrogate and fine model, $< 3\%$ (calculated under l-1 norm).

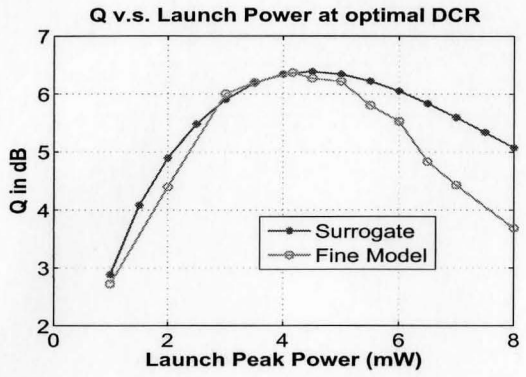

Figure 4.9: Q-factor comparison between the fine and surrogate models at optimal DCR.

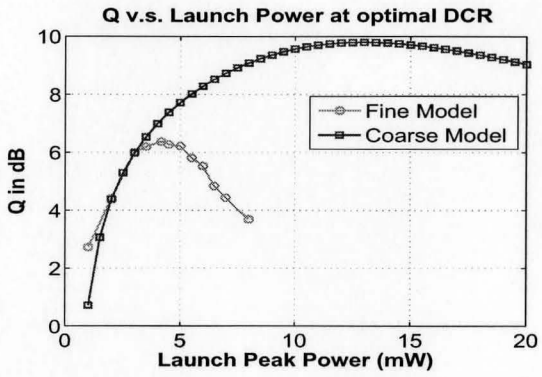

Figure 4.10: Q-factor comparison between the fine and coarse models at optimal DCR.

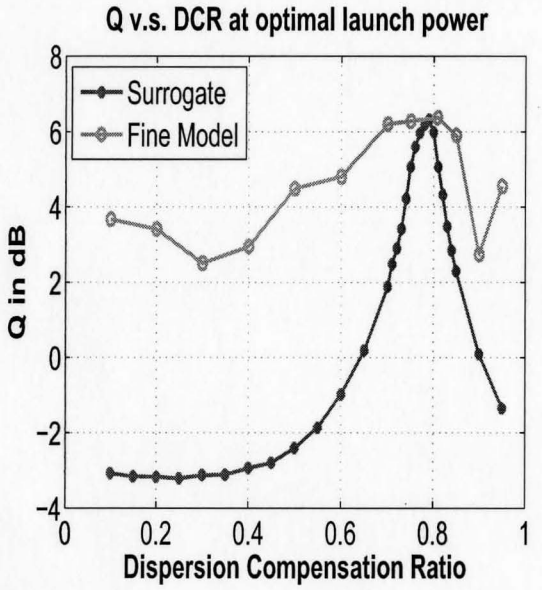

Figure 4.11: Q-factor comparison between the fine and surrogate models at optimal launch power.

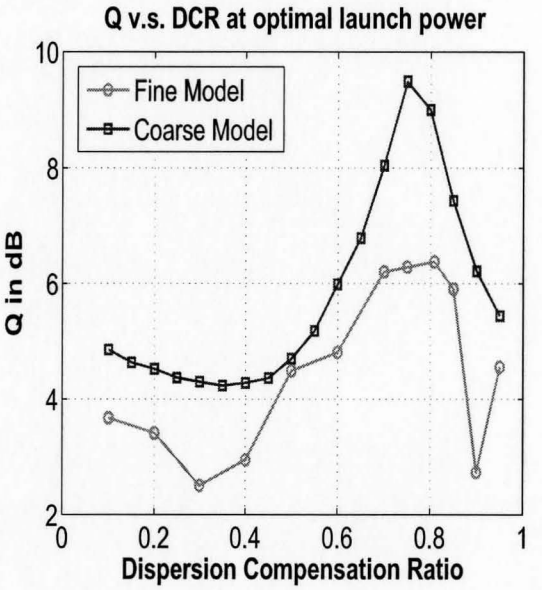

Figure 4.12: Q-factor comparison between the fine and coarse models at optimal launch power.

Chapter 5

Conclusions

In this work, we study the effect of the dispersion slope on fiber-optic transmission systems with two different dispersion maps. We investigate whether it is necessary to compensate the third-order or not and compare the system performance between the schemes having different local dispersions.

Our results show that for the system scheme with the dispersion map consisting of a single transmission (scheme 2, see Fig. 3.2), around $1.8dB$ drop in Q occurs if the third-order dispersion is not compensated, whereas, for the system scheme with the dispersion map consisting of a dispersion managed fiber (scheme 1, see Fig. 3.1), nearly the same performance is achieved for the systems with and without dispersion slope compensation. Therefore, we conclude that it is not a must to compensate the dispersion slope for scheme 1 when the launch power and pre-compensation are all optimized while for scheme 2, it is important to compensate the dispersion slope. Moreover, the impact of the local dispersion is also investigate and the results show that the system performance increases by $\sim 0.8dB$ in Q with higher local dispersion.

We introduce Space Mapping (SM) technique into fiber-optic communications to solve the time-consuming problem in direct optimization and present how to set up a fine and coarse model, how to implement the specific SM algorithms to fine the optimal design parameters. We discuss what benefits we can obtain and what deficiencies we have to

overcome in this application of SM technique.

From our simulations, we find that the SM-based optimization is much better than the direct optimization due to its less computational effort. First, the SM-based optimization is of high efficiency. Only 18 hours are needed to get the optimal design parameters for the SM-based optimization while for the direct optimization, it takes 137 hours or about 5 days. Second, the SM-based optimization can guarantee high accuracy. The relative error between the optima achieved from the surrogate and the fine model is less than 3%. Therefore, we conclude that SM technique can be applied to fiber-optic communications and it effectively reduces the elapsed optimization time, and hence provide us a highly efficient method to get the optimal design parameters.

Finally, there are still some areas we can go into in future work such as how to improve our coarse model and further make the SM algorithm more stable and how to keep the SM-based optimization work well when more design parameters are added in, etc..

Appendix A

Auxiliary Method for Solving NLS

Taking the Fourier transform of (4.12), we have

$$\frac{d\tilde{f}(z,\omega)}{dz} - \frac{j\omega^2\beta_2(z)}{2}\tilde{f}(z,\omega) = -j\tilde{F}(z,\omega) \tag{A.1}$$

where $\tilde{f}(z,\omega)$ is the Fourier transform of $f(z,T)$ and

$$\begin{aligned}\tilde{F}(z,\omega) &= \eta(z)\exp\left(-\sum_{l=1}^{2} C_l^2 R_l\right) \\ &\quad \times \int_{-\infty}^{\infty} \exp[-RT^2 - jT(C_3 + 2jC_r - \omega)]dT \\ &= \frac{\sqrt{\pi}\eta'}{\exp}\left[\frac{-\omega^2}{4R} - \omega D\right]\end{aligned} \tag{A.2}$$

where

$$R = R_1 + R_2, \quad C_r = C_1R_1 + C_2R_2 \tag{A.3}$$

$$D = \frac{-(C_3 + 2jC_r)}{2R} \tag{A.4}$$

$$\eta' = \eta\exp\left(-\sum_{l=1}^{2} C_l^2 R_l + \frac{4C_r^2 - C_3^2 - 4jC_3C_r}{4R}\right) \tag{A.5}$$

The solution of (A.1) with the initial condition $\tilde{f}(0,\omega) = 0$ is

$$\tilde{f}(z,\omega) = -j\int_0^z \tilde{F}(s,\omega)\exp\left[\frac{j\omega^2 A(z,s)}{4}\right]ds \tag{A.6}$$

where

$$\begin{aligned} A(z,s) &= 2[S(z) - S(s)] \\ S(z) &= \int_0^z \beta_2(s)ds \end{aligned} \tag{A.7}$$

Inserting (A.2) into (A.6) and inverse Fourier transforming, we obtain

$$\begin{aligned} f(z,T) &= \frac{-j\sqrt{\pi}}{2\pi} \int_0^z \frac{\eta'(s)}{\sqrt{R(s)}} \\ &\quad \times \int_{-\infty}^{\infty} \exp[-\omega^2\delta/4 - \omega(D + jT)]d\omega ds \end{aligned} \tag{A.8}$$

where

$$\delta(z,s) = \frac{1}{R(s)} - jA(z,s) \tag{A.9}$$

After evaluating the inner integral in (A.8), we obtain

$$f(z,T) = -j \int_0^z \frac{\eta'(s)}{\sqrt{\delta(z,s)R(s)}} \exp\left[\frac{(D(s) + jT)^2}{\delta(z,s)}\right] ds \tag{A.10}$$

Using (A.3)-(A.5) and (A.10), after some algebra, we arrive at (4.14)

Bibliography

[1] Bob Jopson and Alan Gnauck, Disperson Compensation for Optical Fiber Systems, IEEE Communicaitions Magazine, pp. 96-102, June 1995.

[2] Beate Konrad, Anes Hodzic, Klaus Petermann, Dispersion Compensation Schemes for 160 Gb/s TDM-Transmission over SSMF and NZDSF, Proc. 27th Eur.Conf. on Opt. Comm. (ECOC'01 - Amsterdam), pp. 188-189.

[3] Beate Konrad, Klaus Petermann, Jorn Berger, Reinhold Ludwig, Carl Michael Weinert, Hans G. Weber, and Bernhard Schmauss, Impact of Fiber Chromatic Dispersion in High-Speed TDM Transmission Systems, Journal of Ligthwave Technology, Vol. 20, No. 12, Decemeber 2002.

[4] M.Murakami, T.Matsuda, and T.Imai, FWM Generation in Higher Order Fiber Dispersion Managed Transmission Line, IEEE Photonics Technology Letters, Vol. 14, No. 4, April 2002.

[5] Hidenori Tage, Masatoshi Suzuki, Noboru Edagawa, Shu Yamamoto and Shigeyuki Akiba, Long-Distance WDM Transmission Experiments using the Dispersion Slope Compensator, IEEE Jounal of Uqantum Electronics, Vol. 34, No. 11, November 1998.

[6] Michael Otto and Marko Mailand, Dispersion-Compensation Module Based on One Preform Design Matching Arbitrary Dispersion and Slope Requirements, Journal Lightwave Thechnology, Vol. 23, No. 11, November 2005.

[7] Erik Hellström, Henrik Sunnerud, Mathias Westlund and Magnus Karlsson, Third-Order Dispersion Compensation Using a Phase Modulator, Journal of Lightwave Technology, Vol. 21, No. 5, May 2003.

[8] Pavel Ivanoff Reyes, Natalia Litchinitser, Mikhail Sumetsky and Paul S. Westbrook, 160-Gb/s Tunable Dispersion Slope Compensator Using a Chirped Fiber Bragg Grating and a Quadratic Heater, IEEE Photonics Technology Letters, Vol. 17, No. 4, April 2005.

[9] C. C. Chang, H. P. Sardesai, A. M. Weiner, OFC'98 Technical Digest, pp. 75-76.

[10] M. Kato, N. Yoshizawa, T. Sugie and K. Okamoto, Dispersion Slope Equaliser Using Bend-Induced Positive Dispersion Slope in Coiled Pure-Silica Fibre, Electronics Letters, Vol. 37, No. May 24, 2001.

[11] K. Takiguchi, S, Kawanishi, H. Takara, O. Kamatani, K. Uchiyama, A. Himeno and K. Jinguji, Dispersion Slope Equalising experiment Using Planar Lightwave Circuit for 200Gbit/s Time-Division Multiplexed Transmission, Electronics Letters, Vol. 32, No. 22, October 24, 1996.

[12] Fariborz Mousavi Madani and Kazuro Kikuchi, Performance Limit of Long-Distance WDM Dispersion-Managed Transmission System Using Higher Order Dispersion Compensation Fibers, IEEE Photonics Technology Letters, Vol. 11, No. 5, May 1999.

[13] V. Srikant, Broadband Dispersion and Dispersion Slope Compensation in High Bit Rate and Ultra Long Haul Systems, OFC 2001.

[14] John W. Bandler, Radoslaw M. Biernacki, Shao Hua Chen, Piotr A. Grobelny, and Ronald H. Hemmers, Space Mapping Technique for Electromagnetic Optimization, IEEE Transactions on Microwave Theory and Techniques, Vol. 42, No. 12, December 1994.

[15] John W. Bandler, Qingsha S. Cheng, Sameh A. Dakroury, Ahmed S. Mohamed, Mohamed H. Bakr, Kaj Madsen and Jacob Søndergaard, Space Mapping: The State of the Art, IEEE Transactions on Microwave Theory and Techniques, Vol. 52, No. 1, January 2004.

[16] John W. Bandler, Qingsha S. Cheng, Natalia K. Nikolova, and Mostafa A. Ismail, Implicit Space Mapping Optimization Expoiting Preassigned Parameters, IEEE Transactions on Microwave Theory and Techniques, Vol. 52, No. 1, January 2004.

[17] John W. Bandler, Daniel M. Hailu, Kaj Madsen and Frank Pedersen, A Space-Mapping Interpolating Surrogate Algorithm for Highly Optimized EM-Based Design of Microwave Devices, IEEE Transactions on Microwave Theory and Techniques, Vol. 52, No. 11, November 2004.

[18] G. P. Agrawal, Nonlinear Fiber Optics. San Diego, CA: Academic, 1995, ch.3 and 7.

[19] Intrachannel Nonlinear Penalties in Dispersion-Managed Transmission Systems, by Shiva Kumar, John C. Mauro, Srikanth Raghavan and Dipak Q. Chowdhury on IEEE Journal of Selected Topics in Quantum Electronics, 2002.

[20] Shiva Kumar and Dong Yang, Second-Order Theory for Self-Phase Modulation and Cross-Phase Modulation in Optical Fibers, Journal of Lighwave Technology, Vol. 23, No. 6, June 2005.

[21] Sascha Vorbeck and Ralph Leppla, Dispersion and Dispersion Slope Tolerance of 160-Gb/s Systems, Considering the Temperature Dependence of Chromatic Dispersion, IEEE Photon. Tech. Lett., Vol.15, No. 10, October 2003

[22] G.P.Agrawal, Fiber-Optic Communication Systems, 1997

[23] P.V.Mamyshev and N.A.Mamysheva, Pulse-overlapped dispersion-managed data transmission and intrachannel four-wave mixing, Opt. Lett., Vol. 24, No. 21, November 1, 1999.